



저작자표시-비영리-변경금지 2.0 대한민국

이용자는 아래의 조건을 따르는 경우에 한하여 자유롭게

- 이 저작물을 복제, 배포, 전송, 전시, 공연 및 방송할 수 있습니다.

다음과 같은 조건을 따라야 합니다:



저작자표시. 귀하는 원저작자를 표시하여야 합니다.



비영리. 귀하는 이 저작물을 영리 목적으로 이용할 수 없습니다.



변경금지. 귀하는 이 저작물을 개작, 변형 또는 가공할 수 없습니다.

- 귀하는, 이 저작물의 재이용이나 배포의 경우, 이 저작물에 적용된 이용허락조건을 명확하게 나타내어야 합니다.
- 저작권자로부터 별도의 허가를 받으면 이러한 조건들은 적용되지 않습니다.

저작권법에 따른 이용자의 권리는 위의 내용에 의하여 영향을 받지 않습니다.

이것은 [이용허락규약\(Legal Code\)](#)을 이해하기 쉽게 요약한 것입니다.

[Disclaimer](#)

Master's Thesis
석사 학위논문

Field-free magnetization switching and induced
exchange bias by spin torque in $\text{Co}_{0.7}\text{-Ni}_{0.3}\text{-O-Pt}$
phase alloy single layer

Tae-Hwan Kim(김 태 환 金 兌 桓)

Department of
Emerging Materials Science

DGIST

2021

Master's Thesis
석사 학위논문

Field-free magnetization switching and induced
exchange bias by spin torque in $\text{Co}_{0.7}\text{-Ni}_{0.3}\text{-O-Pt}$
phase alloy single layer

Tae-Hwan Kim(김 태 환 金 兌 桓)

Department of
Emerging Materials Science

DGIST

2021

Field-free magnetization switching and induced
exchange bias by spin torque in $\text{Co}_{0.7}\text{-Ni}_{0.3}\text{-O-Pt}$
phase alloy single layer

Advisor: Professor Jung-Il Hong
Co-advisor: Professor Chun-Yeol You

by

Tae-Hwan Kim
Department of Emerging Materials Science
DGIST

A thesis submitted to the faculty of DGIST in partial fulfillment of the requirements for the degree of Master of Science in the Department of Emerging Materials Science. The study was conducted in accordance with Code of Research Ethics 1

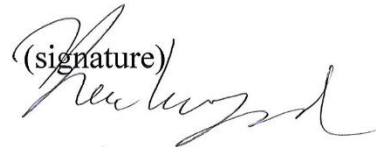
11. 23. 2020

Approved by

Professor Jung-Il Hong
(Advisor)

Professor Chun-Yeol You
(Co-Advisor)

(signature)


(signature)


1 Declaration of Ethical Conduct in Research: I, as a graduate student of DGIST, hereby declare that I have not committed any acts that may damage the credibility of my research. These include, but are not limited to: falsification, thesis written by someone else, distortion of research findings or plagiarism. I affirm that my thesis contains honest conclusions based on my own careful research under the guidance of my thesis advisor.

Field-free magnetization switching and induced
exchange bias by spin torque in $\text{Co}_{0.7}\text{-Ni}_{0.3}\text{-O-Pt}$
phase alloy single layer

Tae-Hwan Kim

Accepted in partial fulfillment of the requirements for the degree of Master of
Science.

11. 23. 2020

Head of Committee Prof. Jung-Il Hong  (signature)

Committee Member Prof. Chun-Yeol You  (signature)

Committee Member Prof. Jungpil Seo  (signature)

MS/EM
201921005

김 태 환. Tae-Hwan Kim. Field-free magnetization switching and induced exchange bias by spin torque in $\text{Co}_{0.7}\text{-Ni}_{0.3}\text{-O-Pt}$ phase alloy single layer. Department of Emerging materials and Science. 2021. 68p. Advisors Prof. Jung-Il Hong, Co-Advisors Prof. Chun-Yeol You.

ABSTRACT

The spin Hall effect has been attracting worldwide attention as one of the methods for controlling the magnetic spin structure. However, it has the limitations in layered structure and requirement of high current density, $J_c \sim 10^{10} \text{A/m}^2$.

In this thesis, the $\text{Co}_{0.7}\text{-Ni}_{0.3}\text{-O-Pt}$ phase alloy single layer having a structure in which each phase is randomly distributed in several nanometer sizes like the alloy was reported. Unlike general layered thin film system, this structure has a unique interfacial structure as Co, Ni, O and Pt phases are randomly distributed in a single layer.

When a current is applied to this thin film, the spin Hall effect generated by the current flowing through the Pt phases applies spin torque to other phases at the interface, and this result was observed through the change of the exchange bias. To find out the cause of the occurrence, the same structure was fabricated using Au instead of Pt and Fe instead of Co and Ni, and the same experiment was performed. As a result, it was found that the spin structure of the antiferromagnetic material was controlled by the spin Hall effect. In addition, the magnitude of the induced exchange bias was proportional to the current density and degree of oxidation of the film and exhibited stable reversibility and repeatability within the measured current density range. Using this, field-free magnetization switching was also performed and all of the results were achieved at a current density of $J_c \sim 10^{10} \text{A/m}^2$, which is one order lower than the previously reported value.

Therefore, the results of this thesis overcome the limitations of the spin torque and the layered thin film system through phase alloy single layer structure, which suggests the possibility of improving the performance of a device designed based on the control of the spin structure.

Keywords: spin torque, spin Hall effect, switching

List of Contents

Abstract	i
List of contents	ii
List of tables	iv
List of figures	v
I . Introduction	1
I I . Theoretical Background	3
2.1 Magnetism	3
2.1.1 Ferromagnetism	3
2.1.2 Antiferromagnetism	6
2.2 Exchange interaction	8
2.3 Exchange bias	9
2.4 Spin-orbit interaction	11
2.5 Spin Hall effect	13
2.6 Spin torque	16
I I I . Experimental Details	18
3.1 Fabrication Co _{0.7} -Ni _{0.3} -O-Pt Phase alloy single layer	18
3.1.1 Metal-metal oxide phase mixture	18
3.1.2 Reactive magnetron co-sputtering	20
3.1.3 Photolithography	23
3.2 Structural property measurement	25
3.2.1 X-ray Diffraction(XRD)	25
3.2.2 Transmission Electron Microscopy(TEM)	26
3.2.3 Scanning Electron Microscope(SEM)	27
3.3 Magnetic property measurement	28
3.3.1 Vibrating Sample Magnetometer(VSM)	28
3.3.2 Magneto-Optical Kerr Effect microscopy(MOKE)	29

IV. Results and Discussion	31
4.1 Characterization of Co _{0.7} -Ni _{0.3} -O-Pt phase alloy single layer	31
4.1.1 Confirm the degree of oxidation	31
4.1.2 Crystal structure of Co _{0.7} -Ni _{0.3} -O-Pt depending on degree of oxidation	33
4.2 Controlled magnetic properties by spin Hall effect	39
4.2.1 Aligned AFM and interface effect through spin Hall effect	39
4.2.2 Magnitude of induced exchange bias depending on oxidation degree and current density	44
4.2.3 Reversible and repeatable exchange bias depending on direction of charge current	46
4.2.4 Field-free magnetization switching	50
V. Conclusion	52
VI. Reference	53

List of tables

Table 1. Magnitude of Curie temperature and saturation magnetization of Fe, Co and Ni

Table 2. Magnitude of spin Hall angle of Pt, Au and Ta

Table 3. Magnitude of saturation magnetization and oxidation degree of $\text{Co}_{0.7}\text{-Ni}_{0.3}\text{-O-Pt}$ phase alloy single layer depending on oxygen flow rate

List of Figures

Figure. 1 Spin alignment of ferromagnetic material depending on external magnetic field

Figure. 2 (a) Typical hysteresis loop and (b) temperature dependence of magnetic moment of ferromagnetic material

Figure. 3 Spin alignment of antiferromagnetic material

Figure. 4 Susceptibility of ferro, para and antiferro magnetic material depending on temperature

Figure. 5 (a), (b) typical spin structure and interfacial exchange coupling and (c),(d) hysteresis loop and exchange bias field (H_E) depending on temperature of FM/AFM bilayer

Figure. 6 Schematic of spin-orbit interaction (a) orbiting nucleus around fixed electron creates effective magnetic field (\vec{B}), (b) spin angular momentum (\vec{S}) caused by electron spinning motion, interaction between nucleus and (c) up-spin and (d) down-spin, respectively.

Figure. 7 Schematic of spin Hall effect

Figure. 8 Illustration of unpolarized current, spin polarized current, fully spin polarized current and pure spin current depending on polarized spin electron moving

Figure. 9 Schematic of spin torque caused by spin Hall effect in magnetic/non-magnetic heavy metal bilayer.

Figure. 10 XRD patterns of phase mixture films for $\text{Co}_{0.7}\text{Ni}_{0.3}$ - $\text{Co}_{0.7}\text{Ni}_{0.3}\text{O}$ with degree of

oxidation varying from 0 to 97%

Figure. 11 Atom probe tomograph image of Co-CoO phase mixture film with 43% oxidation degree

Figure. 12 Magnetic properties depending on the oxidation ratio in $\text{Co}_{0.7}\text{Ni}_{0.3}$ - $\text{Co}_{0.7}\text{Ni}_{0.3}\text{O}$ mixture films with temperature. (a) Hysteresis loops of the film with 48% oxidation content at temperatures from 10K to 325K. (b) The change of M_s depending on the temperature. (c) The change of ΔM_s between 325K and 10K. (d) Schematic view of the expected spin structures depending on temperature at the interface between FM and AFM.

Figure. 13 Schematic of reactive magnetron co-sputtering using $\text{Co}_{0.7}\text{Ni}_{0.3}$ and Pt target for fabricating the $\text{Co}_{0.7}\text{-Ni}_{0.3}\text{-O-Pt}$ phase alloy single layer

Figure. 14 Process of photolithography for fabricating patterned thin film.

Figure. 15 Schematic diagram of MOKE measurement.

Figure. 16 Hall bar pattern for applying high current density with $10\mu\text{m}$ width and $40\mu\text{m}$ length in one leg. Direction of applied current and external magnetic field is represented by yellow and red arrow, respectively. Blue circle region is measured by MOKE.

Figure. 17 XRD patterns of (a) Pt and (b) Au film deposited in $\text{Ar} + \text{O}_2$ (0.9sccm) atmosphere.

Figure. 18 (a) XRD patterns of $\text{Co}_{0.7}\text{-Ni}_{0.3}\text{-O-Pt}$ phase alloy single layers depending on oxidation degree and (b) enlarged XRD pattern to confirm the decline of crystallinity

Figure. 19 FWHM(full width half maximum) of $\text{Co}_{0.7}\text{-Ni}_{0.3}\text{-O-Pt}$ (111) peak and crystallite size depending on oxidation degree

Figure. 20 TEM image of (a) 0% oxidation degree and (b) oxidation degree of $\text{Co}_{0.7}\text{-Ni}_{0.3}\text{-O-Pt}$ films. Yellow line and rectangle represent the crystalline and grain boundary, respectively.

Figure. 21 Atomic mapping image measured by TEM of 82% oxidation degree $\text{Co}_{0.7}\text{-Ni}_{0.3}\text{-O-Pt}$ phase alloy single layer.

Figure. 22 Hysteresis loops measured by MOKE of (a) 0%, (b) 82% oxidation degree of $\text{Co}_{0.7}\text{-Ni}_{0.3}\text{-O-Pt}$, (c) 78% oxidation degree of $\text{Co}_{0.7}\text{-Ni}_{0.3}\text{-O-Au}$ and (d) 79% oxidation degree of Fe-O-Pt phase alloy. Black line is measured without current and red line is measured during applying current.

Figure. 23 Magnitude of induced exchange bias depending on current density of phase alloy single layers.

Figure. 24 Magnitude of induced exchange bias depending on current density and oxidation degree of $\text{Co}_{0.7}\text{-Ni}_{0.3}\text{-O-Pt}$ phase alloys.

Figure. 25 Resistance of $\text{Co}_{0.7}\text{-Ni}_{0.3}\text{-O-Pt}$ phase alloy single layer depending on oxidation degree

Figure. 26 Hysteresis loops of 82% oxidized $\text{Co}_{0.7}\text{-Ni}_{0.3}\text{-O-Pt}$ when $J_c = \pm 4.62 \times 10^{10} \text{ A/m}^2$ is repeatedly applied.

Figure. 27 Magnitude of induced exchange bias of 82% oxidized $\text{Co}_{0.7}\text{-Ni}_{0.3}\text{-O-Pt}$ when $J_c = \pm 4.62 \times 10^{10} \text{ A/m}^2$ is repeatedly applied.

Figure. 28 Magnitude of induced exchange bias of 68% and 82% oxidized $\text{Co}_{0.7}\text{-Ni}_{0.3}\text{-O-Pt}$ by

sweeping current density.

Figure. 29 Hysteresis loops of 82% oxidized $\text{Co}_{0.7}\text{-Ni}_{0.3}\text{-O-Pt}$ phase alloy single layer when current is applied, $J_c = \pm 4.2 \times 10^{10} \text{ A/m}^2$. Magnetic moment is aligned in same direction by induced exchange bias at H_{ext} is zero regardless of sweeping direction.

Figure. 30 Magnetic domain images. (a) and (d) are saturated by external field in \pm direction before applying current, (b) and (e) are switched by spin torque caused by spin Hall effect in opposite directions. (c) and (f) represent remanence magnetization formed in the switched direction

I . INTRODUCTION

In the field of spintronics, controlling magnetic properties such as spin structure of magnetic materials has become an important issue for many years and many applications such as hard disk¹ and MRAM^{2,3}. In addition to this, the methods of controlling magnetic properties are also a very important factor because various conditions such as heat, amount of current, external magnetic field and voltage must be considered. In recent studies, many researchers have attempted to adjust the spin structure of not only ferro magnet (FM)^{4,5,6} but also anti-ferro magnet (AFM) through spin torque without a need to apply heat treatment and external magnetic field^{7,8}. As a source generating spin torque to control the spin structure, the spin current generated by the spin Hall effect is attracting worldwide attention^{9,10,11,12}. In the case of AFM, although it is difficult to control the spin structure compared to ferro magnet (FM) due to low susceptibility¹³. It was reported that spin structure of NiO was controlled by spin current and it leads to change of resistance³. In addition, through several results¹⁴, it was revealed that spin torque caused by spin Hall effect is an effective method for controlling spin structure of AFM.

Spin Hall effect (SHE) is caused by charge current flowing heavy-metal layer with large spin-orbit coupling (SOC) and make the polarized spins split to opposite direction^{15,16}. Spin current caused by the polarized spins can be injected to neighboring magnetic layers. The injected spin current can interact with spins and rotate spin direction of neighboring magnetic layers, which is called the ‘spin torque’¹⁷. To effectively control the spin structure of magnetic layer using spin torque caused by spin Hall effect, the strength and direction of spin current must be considered. Spin Hall angle of heavy-metal layer and direction and density of

charge current are the main factors determining the direction and amount of spin current. The amount of spin current is proportional to charge current density flowing through heavy metal layer and spin Hall angle of heavy metal layer. Considering thermal effect and power consumption in terms of spintronics, large spin Hall angle and low current density are preferred. To confirm the controlled spin structure by spin current, there are several methods such as magnetic domain, change of resistance and exchange bias.

Direction and magnitude of exchange bias caused by interfacial exchange coupling between FM and AFM materials can be controlled by many methods such as field cooling^{18,19} and spin torque^{20,21}. Unlike field cooling, which requires heat treatment to make the temperature of AFM layer above the Neel temperature, spin torque method through SHE can control Neel axis of AFM layer^{9,10}. But there are several issues due to the layered film structure such as generation of oersted field by electrical current and the limitation of spin diffusion length of spin current caused by SHE²², and it still requires large current density over 10^{11} A/m².⁹

In this thesis, we fabricate the Co_{0.7}-Ni_{0.3}-O-Pt phase alloy single layer structure to overcome mentioned issues. The Co_{0.7}-Ni_{0.3}-O phase alloy single layer structure was reported as a structure in which FM(Co_{0.7}Ni_{0.3}) and AFM(Co_{0.7}Ni_{0.3}O) are co-existing and randomly distributed in a few nanometer size in single layer²³. Because of this structural characteristic, the large interfacial density and effect between FM and AFM is expected and reflected as the increase of saturation magnetization(M_s) and exchange bias value depending on temperature^{23,24}. By adding Pt atoms in this structure, we expect that the effect of spin torque caused by spin Hall effect and required current density to control spin structure of AFM will be increased and decreased, respectively. As a result, we adjust the spin structure of AFM using spin torque at $J_c = \sim 10^{10}$ A/m², which is one order lower than reported current density in layered structure, in Co_{0.7}-Ni_{0.3}-O-Pt phase alloy single layer and it was confirmed through changes of exchange bias and magnetic domain.

I I . Theoretical Background

2.1 Magnetism

Magnetism is a class of physical phenomena which are influenced by magnetic field. All materials exhibit some type of magnetism and its type can be classified through its behavior with respect to a magnetic field. The types of magnetism are ferromagnetism, antiferromagnetism, ferrimagnetism, paramagnetism and diamagnetism.

2.1.1 Ferromagnetism

Ferromagnetism refers to the magnetic properties of the materials that have a spin structure aligned in a direction parallel between spins and it is magnetized without external magnetic field such as Fe, Co, and Ni. The virgin magnetization value of ferromagnetic materials with polycrystalline is close to zero because spins are aligned in a parallel direction but each the domains are aligned in random directions like Fig. 1 (a). When an external magnetic field of sufficient size is applied to the ferromagnet materials in this state, the spins are aligned in the direction of external magnetic field as shown in Fig. 1 (b), and the magnetized state in the corresponding direction is maintained even after removing the external magnetic field as shown in Fig. 1 (c). This state is called remanent magnetization. This ferromagnetic property decreases due to thermal fluctuation as the temperature increases, and above curie temperature (T_c), it has a spin array like paramagnetic. When the temperature falls below T_c again, it is arranged like an initial state.

The ferromagnetic property is effectively revealed through the hysteresis loop. When we measure magnetization (or magnetic moment) of ferromagnet during sweeping external magnetic field, we can obtain hysteresis loop like Fig.2(a). The region where all spins are aligned so that the magnetization value no longer increases even when the external magnetic field increases is called saturation magnetization (M_s). The external magnetic field value which become magnetization value is zero is coercivity (H_c).

Fig.2(b) shows the change in magnetization of ferromagnet depending on temperature. Also, saturation magnetization value and curie temperature of Fe, Co, and Ni are shown in the table.1

Material	Curie temperature(K)	M_s(emu/cc) at RT
Fe	1043	1714
Co	1400	1422
Ni	627	484

Table. 1 Magnitude of Curie temperature and saturation magnetization of Fe, Co and Ni

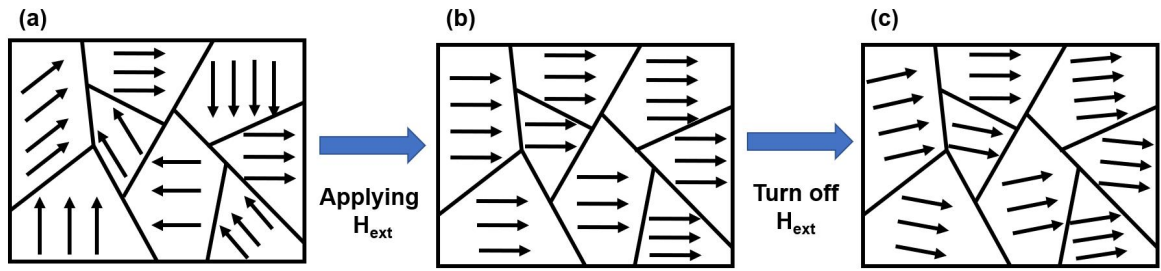


Fig. 1 spin alignment of ferromagnetic material depending on external magnetic field.

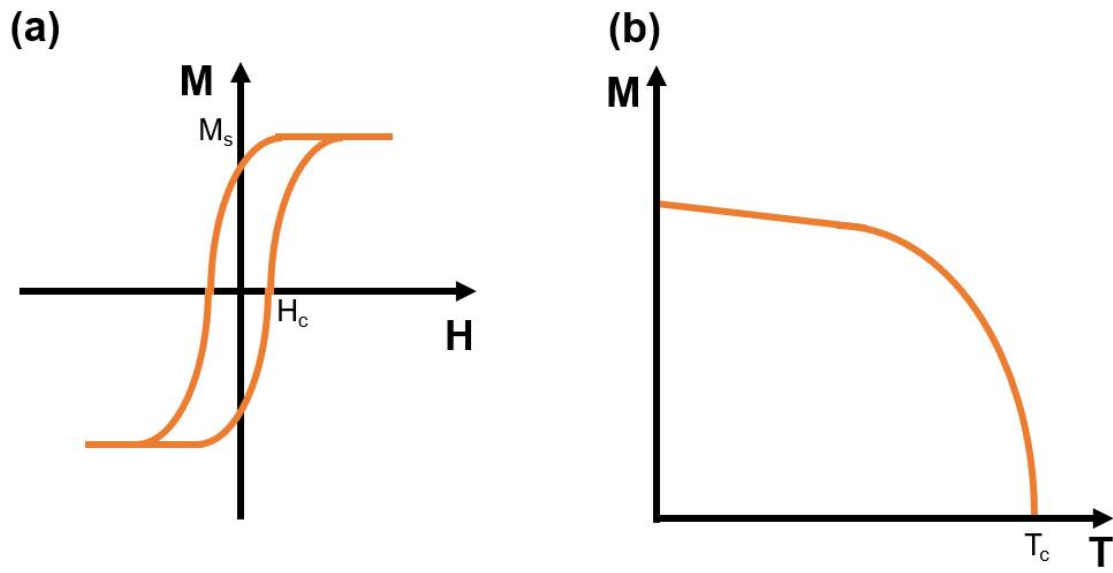


Fig. 2 (a) typical hysteresis loop and (b) temperature dependence of magnetic moment of ferromagnetic material.

2.1.2 Antiferromagnetism

Unlike ferromagnetic materials, the spin structure of antiferromagnetic materials has tendency to arrange the interactions between magnetic moments in an antiparallel direction. As a result, it has spin structure that is antiparallel to each other as shown in Fig. 3 and has a net magnetic moment close to zero.

In addition, as the temperature increases, the spin array becomes unstable due to thermal fluctuation, and it exhibits paramagnetic properties above a certain temperature. This temperature is called Neel temperature (T_N).

In general, antiferromagnetic materials have relatively lower susceptibility than ferromagnet and paramagnet. (Fig. 4) For this reason, it is relatively difficult to control the spin structure of antiferromagnet compared to ferromagnet.

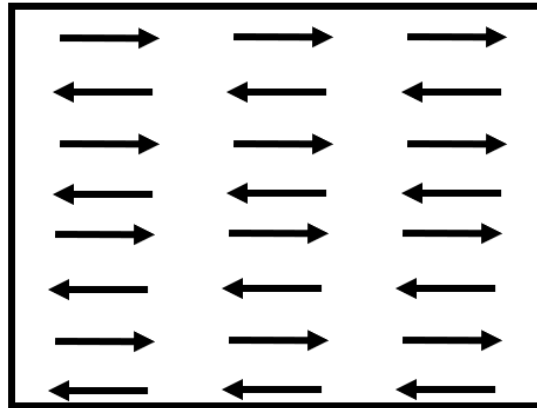


Fig. 3 Spin alignment of antiferromagnetic material

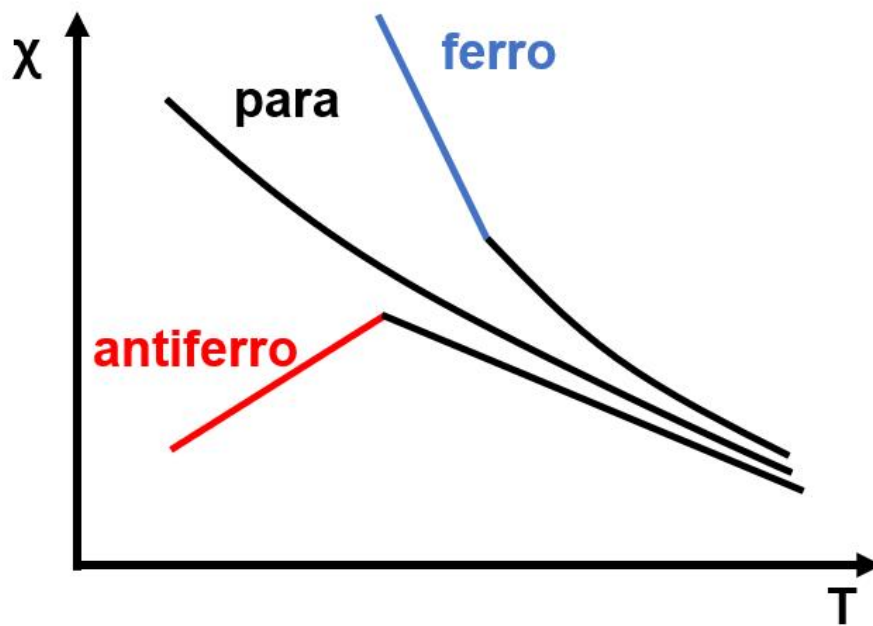


Fig. 4 Susceptibility of ferro, para and antiferro magnetic material depending on temperature

2.2 Exchange interaction

Exchange interaction is an important concept in describing the spin configuration, it is described in quantum mechanics and is related to the Pauli exclusion principle.

In general, the attractive force between atoms separated by a certain distance is mainly described by Coulomb's law. However, there is additionally a force in the spin direction ($+\frac{1}{2}$ or $-\frac{1}{2}$) of electrons, and the concept representing this is exchange interaction, which is well expressed by Pauli exclusion principle.

The relationship between spins can be known through exchange energy. The exchange energy between the two atoms i and j having the spin angular momentum $S_i\hbar/2\pi$ and $S_j\hbar/2\pi$ is expressed as follows.

$$E_{ex} = -2J_{ex}S_iS_j = -2JS_iS_j\cos\phi$$

J_{ex} is the *exchange integral*, which occurs in the calculation of the exchange effect, and ϕ is the angle between the spins. For example, when J_{ex} is positive and E_{ex} is the minimum value, the spins have a parallel ordering. As can be seen from this, the parallel and antiparallel spin alignment of ferromagnet and antiferromagnet is due to exchange interaction.

2.3 Exchange bias effect

Exchange bias is caused by exchange interaction at the interface between ferromagnet and antiferromagnet and shift the hysteresis loop in one direction. The spin of the ferromagnet in the interface region and the spin of antiferromagnet are coupled to each other through exchange interaction. Therefore, the ferromagnet spins of the interface are affected by characteristic that the spin alignment does not change easily with respect to the external magnetic field of the antiferromagnet. As a result, the spin of the interface is pinned, and this effect is called exchange bias.

To get the exchange bias effect effectively, it is necessary to satisfy $T < T_N$ and align the spin structure of the antiferromagnet. As shown in Fig. 5 (a), under $T_N < T$ condition, the spins of antiferromagnet have a random orientation like paramagnet, and if the spins of antiferromagnet are not aligned, the spins of the interface may not be pinned in one direction. A common way to obtain the exchange bias is the field cooling process. It is a method of raising the temperature to $T_N < T < T_c$, then applying an external magnetic field and lowering it back to $T < T_N$. As a result, a spin structure is formed as shown in Fig. 5 (b) and an exchange bias effect appears. Due to the pinned spins, the amount of external magnetic field required for reversing magnetization. In Fig. 5 (c), where there is no exchange bias effect, H_{c1} and H_{c2} are symmetric, whereas in Fig. 5 (d), where there is exchange bias effect, an asymmetric relationship is formed between H_{c1} and H_{c2} . The difference between this asymmetric field value is called exchange bias field (H_E). The magnitude of H_E is as follows

$$H_E = \frac{(H_{c2} - H_{c1})}{2} - H_{c2}$$

The magnitude of the exchange bias in the ferromagnet/antiferromagnet bilayer structure has a simplified relationship as follow.

$$H_E = \frac{\Delta\sigma}{M_{FM}t_{FM}}$$

Where $\Delta\sigma$ is the interfacial unidirectional energy density (erg/cm²) and M_{FM} and t_{FM} are the saturation magnetization and the thickness of ferromagnet material, respectively.

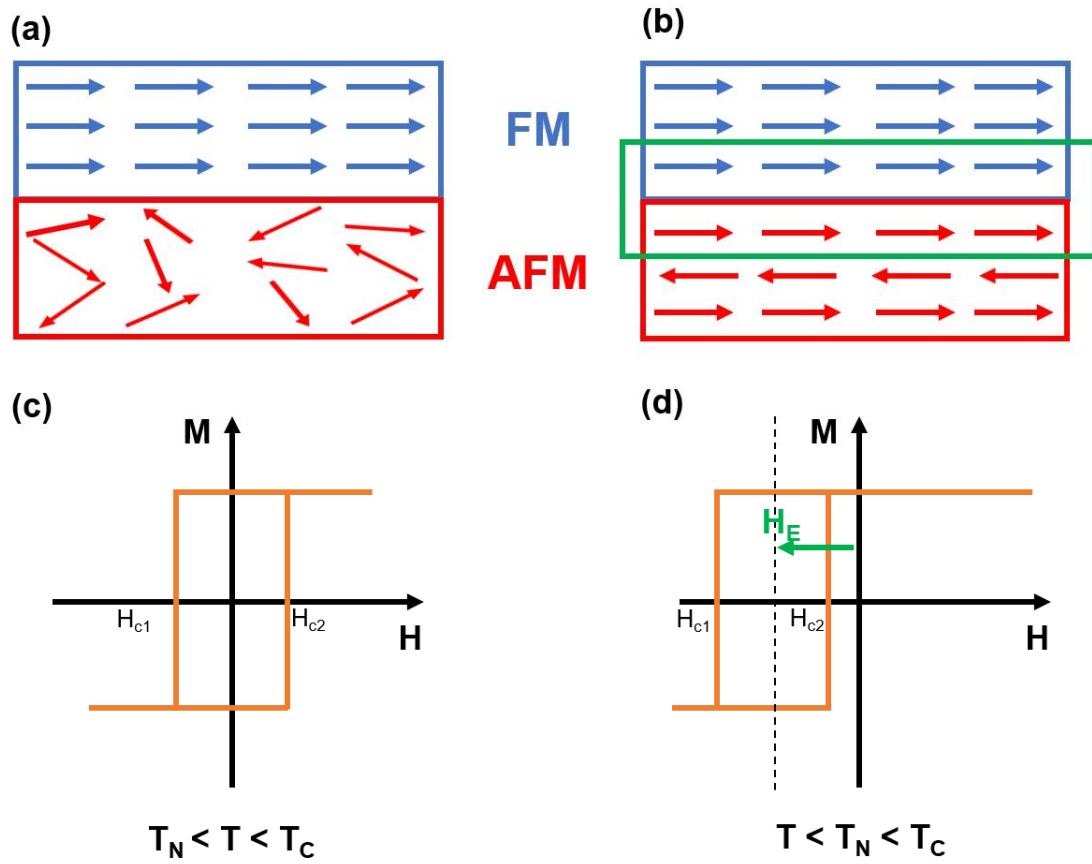


Fig. 5 (a), (b) typical spin structure and interfacial exchange coupling and (c),(d) hysteresis loop and exchange bias field(H_E) depending on temperature of FM/AFM bilayer.

2.4 Spin-orbit interaction

The magnetic moment of the electron spins can interact with the magnetic field generated by electron's orbital motion. The result of this interaction is called spin-orbit interaction or spin-orbit coupling or spin-orbit effect.

From the point of view of an electron fixed in a space, the nucleus of an atom orbits around it as shown in Fig. 6 (a). A current loop is formed by the orbiting nucleus, which induce a effective magnetic field (\vec{B}). The magnetic moment formed by the induced magnetic field is called the orbital angular moment (\vec{L}).

In addition to this, the electron takes a spinning motion by itself as shown in Fig. 6 (b), which induces a magnetic dipole moment (μ_B) and leads to a spin angular moment (\vec{S}).

These two magnetic moments interact with each other, which is called spin-orbit interaction. At this time, the spin magnetic moment receives torque by the magnetic field induced by orbital motion. This torque tries to rotate the spin magnetic moment in the direction of the effective magnetic field.

Fig. 6 (c) and Fig. 6 (d) show the spin-orbit interaction of the up spin and down spin respectively.

Due to this property, a material with a larger atomic number (Z) induces a stronger magnetic field and a strong spin-orbit interaction appears. In fact, it is known that the spin-orbit interaction is proportional to Z^4 .

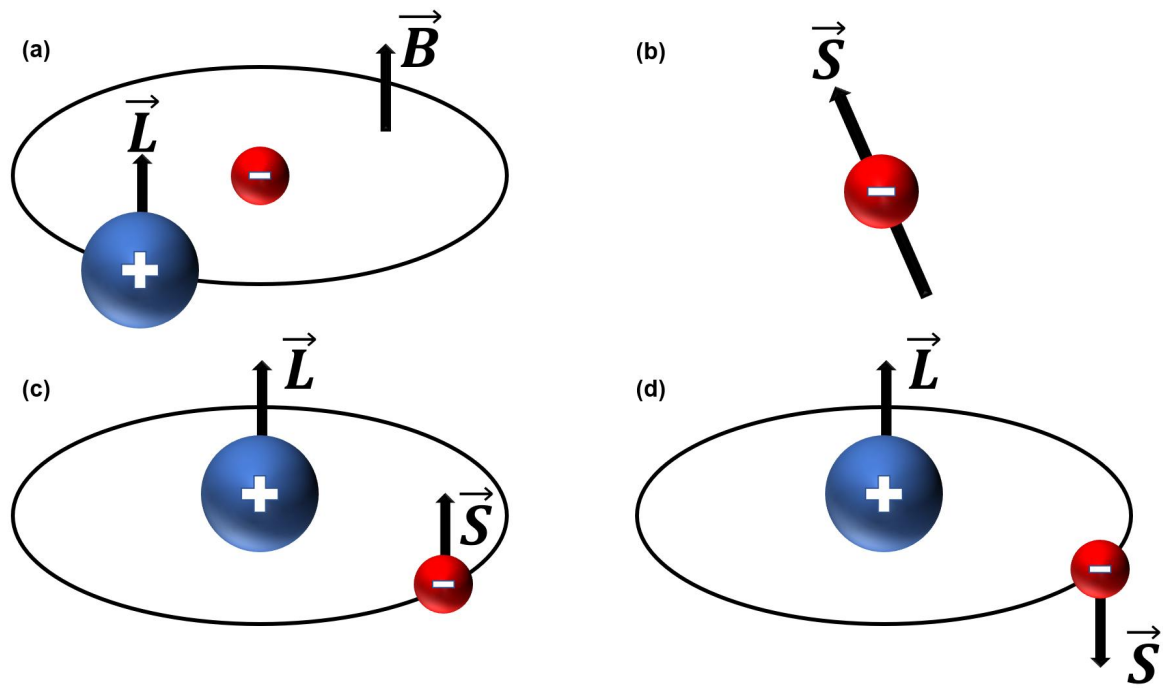


Fig. 6 Schematic of spin-orbit interaction (a) orbiting nucleus around fixed electron creates effective magnetic field (\vec{B}), (b) spin angular moment (\vec{S}) caused by electron spinning motion, interaction between nucleus and (c) up-spin and (d) down-spin, respectively.

2.5 Spin Hall effect

Spin Hall effect is a transport phenomenon that occurs when charge current flows through heavy metal layers which have strong spin-orbit coupling such as Pt and W. By this effect, electrons of charge current applied to the heavy metal layer move in a direction perpendicular to the charge current direction. Unlike the Hall effect, it induces the movement of electrons without an external magnetic field. At this time, the direction of movement changes depending on the spin direction of electron. As a result, spin electrons in different directions move in opposite directions by the same amount as shown in Fig.7. In contrast to the Hall effect in which electrons are biased to one side, the result of the spin Hall effect does not have a difference in potential at both ends. Therefore, no charge current occurs due to the transferred electrons. However, spin current occurs due to the difference in the direction of the moved spins. The difference between the charge current and the spin current depending on the movement of electrons is simply expressed as shown in Fig.8. The spin current generated by the spin Hall effect is expressed by the following equation.

$$J_s = \left(\frac{\hbar}{2e}\right) \theta_{SH} J_c \times \sigma$$

J_s is the spin current, \hbar is the reduced Planck's constant, e is the electron charge, θ_{SH} is the spin Hall angle, J_c is charge current density and σ is the polarization of accumulated spins. The spin Hall angle means conversion efficiency between charge current and spin current. Therefore, the direction of the spin current is determined not only by the direction of charge current but also by the spin Hall angle of the material.

Material	$\theta_{SH}(\%)$
Pt	1.1 ~ 1.5
Au	0.32 ~ 0.38
Ta	-0.5 ~ -3.5

Table. 2 Magnitude of spin Hall angle of Pt, Au and Ta

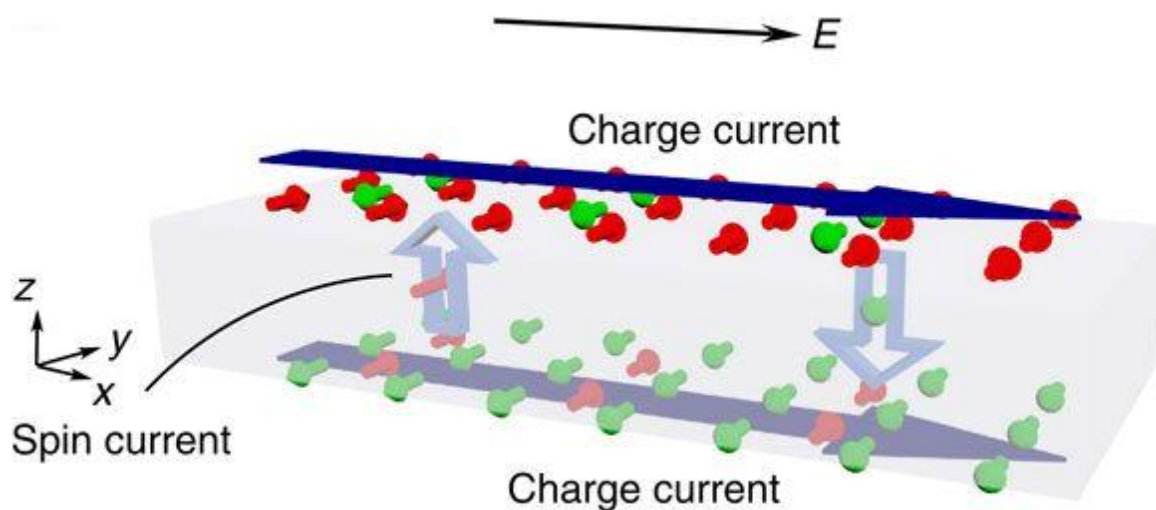


Fig. 7 Schematic of spin Hall effect²⁵

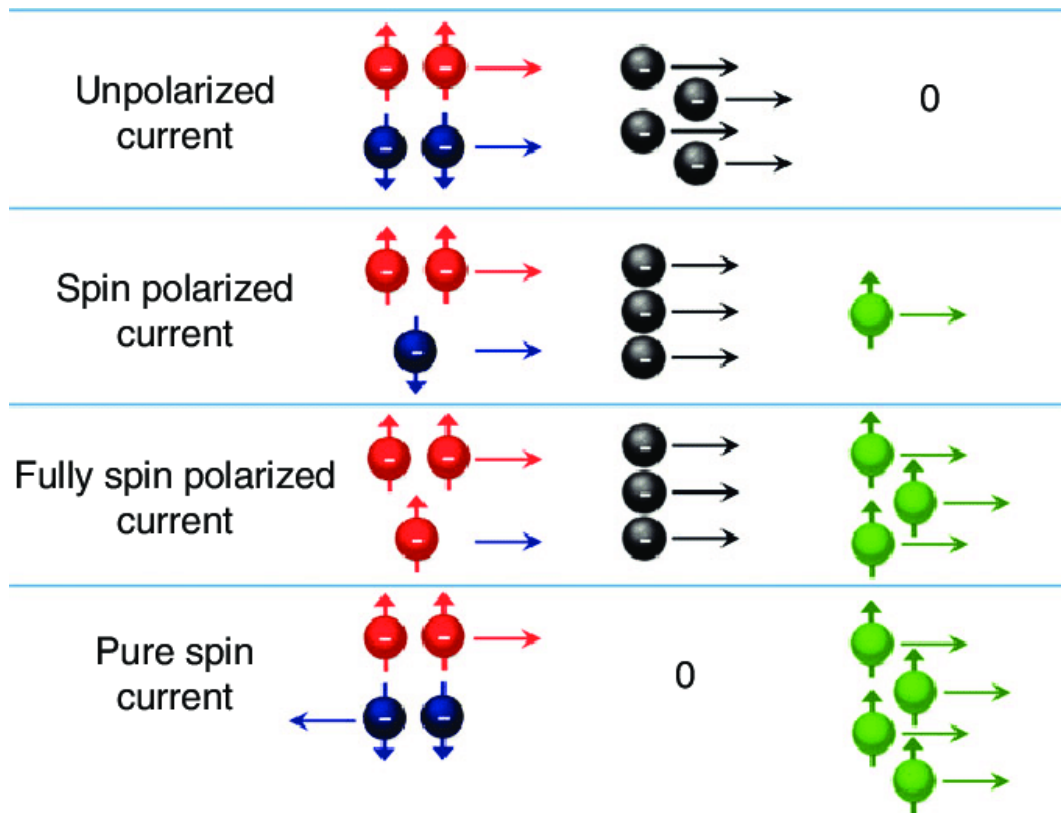


Fig. 8 Illustration of unpolarized current, spin polarized current, fully spin polarized current and pure spin current depending on polarized spin electron moving.²⁶

2.6 Spin torque

The spin current generated by the spin Hall effect can be injected into a neighboring magnetic layer and rotate the spin structure of the magnetic layer. This is called spin torque. Fig.9 shows the spin rotation of the magnetic layer due to the spin torque caused by the spin current. The strength of spin torque is expressed by the following equation.

$$\boldsymbol{\tau} = \mathbf{m} \times \overrightarrow{H_{eff}}$$

$$\overrightarrow{H_{eff}} = -\mathbf{m} \times \boldsymbol{\sigma}$$

$$\boldsymbol{\tau} = -\mathbf{m} \times (\mathbf{m} \times \boldsymbol{\sigma})$$

Therefore, the strength of the spin torque by the spin current is determined by the spin Hall angle and charge current density. At this time, in order to minimize heat generation and power consumption and to control the spin structure using spin torque, it is more advantageous to use a material with a stronger spin Hall angle than to increase the charge current density.

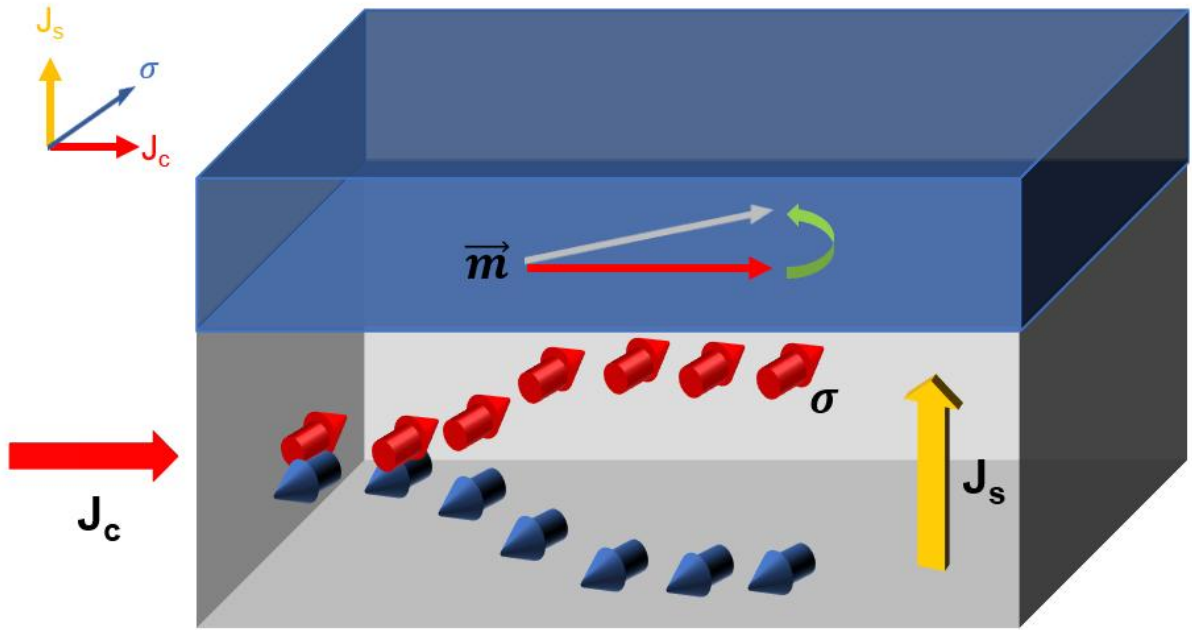


Fig. 9 Schematic of spin torque caused by spin Hall effect in magnetic/non-magnetic heavy metal bilayer.

I I I. Experimental Details

3.1 Fabrication Co_{0.7}-Ni_{0.3}-O-Pt phase alloy single layer

3.1.1 Metal-metal oxide phase mixture

As shown in Fig.10, Co-O phase alloy single layer was reported as a thin film structure with Co pure metal phases (FM) and CoO metal oxide phases (AFM) in a single layer¹⁴. In this structure, pure metal phases and metal oxide phases are randomly distributed. In order to make multiple phases exist simultaneously, a Co pure metal target was deposited by reactive sputtering by controlling the amount of oxygen gas inside chamber. As a result, only a part of the atoms separated from target were oxidized and phase alloy single layer was fabricated.

The size of the phases was affected by the oxidation degree and was formed in nanometer size. As shown in Fig.10, in XRD peak depending on oxidation degree of Co_{0.7}Ni_{0.3}-Co_{0.7}Ni_{0.3}O phase mixture, the intensities of the pure metal (Co_{0.7}Ni_{0.3}) peak and metal oxide (Co_{0.7}Ni_{0.3}O) peak were decreased and increased, respectively, with increase of oxidation degree. The xrd data of 54% and 58% oxidation degree show that the peak has become broad, which means a decline of grain size and crystallinity. Analysis through Scherrer equation²⁷ shows that each phase was formed in a few nanometer sizes.

$$\tau = \frac{K\lambda}{\beta \cos \theta}$$

In Scherrer equation, τ is the mean size of the ordered crystalline domains and K is a dimensionless shape factor, λ is X-ray wavelength, β is the line broadening at half the maximum intensity (FWHM) and θ is the Bragg angle.

In addition, the same result was found in the Co-CoO atom probe tomograph image of Fig. 11. On the other hand, as the oxidation degree continues to increase, the xrd peak becomes sharp again, which means that the AFM ($\text{Co}_{0.7}\text{Ni}_{0.3}\text{O}$) regions become dominant, and grain size and crystallinity are improved.

As a result, the amount of interface between the pure metal (FM) and metal oxide (AFM) phases also changed depending on the degree of oxidation. Because of this structural feature, a larger interface effect occurred compared to the ferromagnet/antiferromagnet bilayer structure, and the interface effect was changed depending on oxidation degree. It was reported through the magnitude of exchange bias²⁴ and the amount of change in saturation magnetization (Ms) depending on temperature.²³ (Fig.12)

In this thesis, we fabricated $\text{Co}_{0.7}\text{-Ni}_{0.3}\text{-O-Pt}$ phase alloy single layer using reactive magnetron co-sputtering technique to take structural advantage of phase alloy single layer. It was expected that spin structure could be effectively controlled by the spin torque generated by the spin Hall effect.

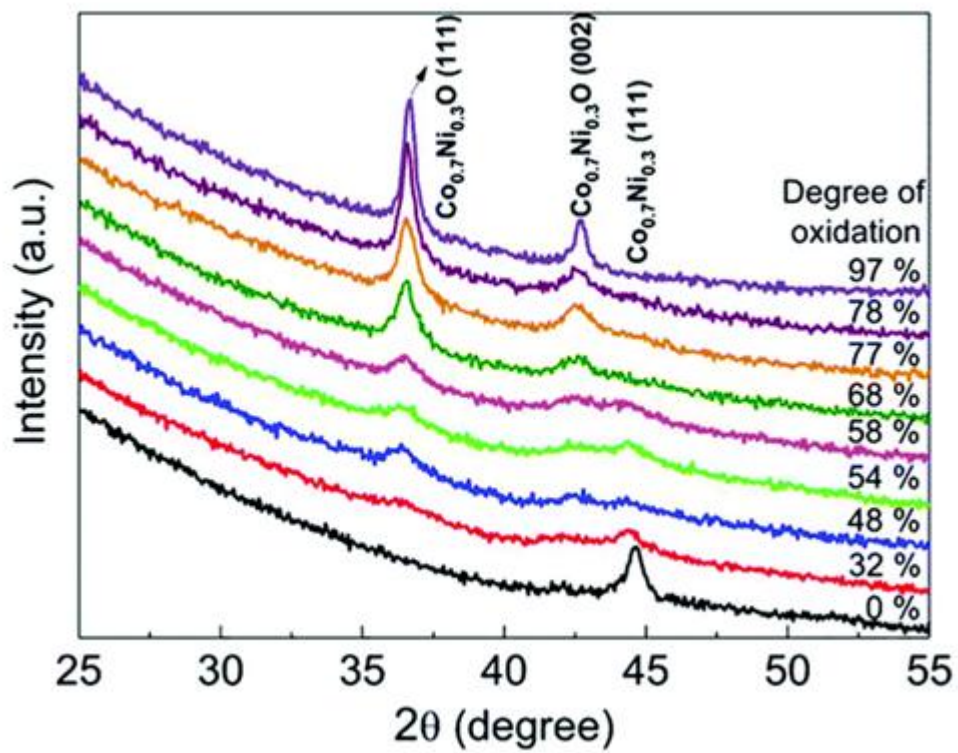


Fig. 10 XRD patterns of phase mixture films for $\text{Co}_{0.7}\text{Ni}_{0.3}$ - $\text{Co}_{0.7}\text{Ni}_{0.3}\text{O}$ with degree of oxidation varying from 0 to 97%.²³

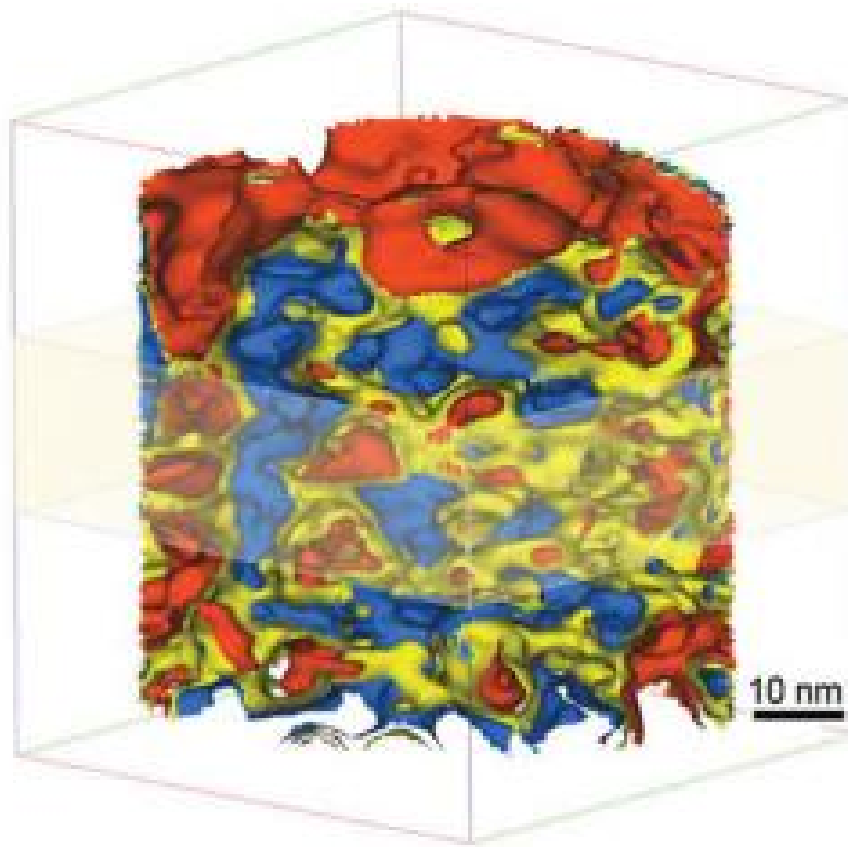


Fig. 11 Atom probe tomograph image of Co-CoO phase mixture film with 43% oxidation degree.²³

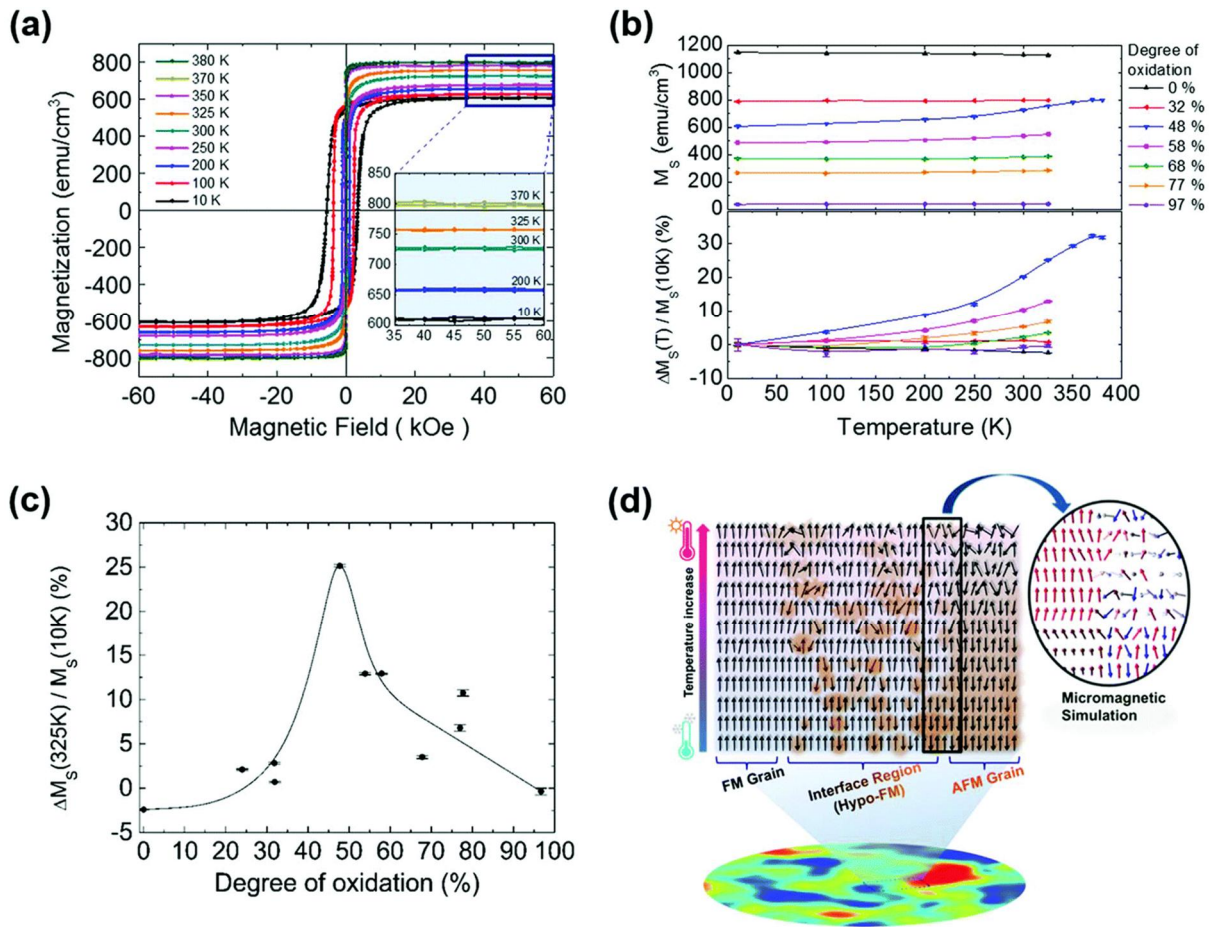


Fig. 12 Magnetic properties depending on the oxidation ratio in $\text{Co}_{0.7}\text{Ni}_{0.3}\text{-Co}_{0.7}\text{Ni}_{0.3}\text{O}$ mixture films with temperature. (a) Hysteresis loops of the film with 48% oxidation content at temperatures from 10K to 325K. (b) The change of M_s depending on the temperature. (c) The change of ΔM_s between 325K and 10K. (d) Schematic view of the expected spin structures depending on temperature at the interface between FM and AFM.²³

3.1.2 Reactive magnetron co-sputtering

In order to fabricate $\text{Co}_{0.7}\text{-Ni}_{0.3}\text{-O-Pt}$ phase alloy single layer, DC magnetron reactive and co sputtering method was used. Sputtering technique is one of the physical vapor deposition methods for producing thin films. In the chamber, a gas ionized by an electric field (in our case, Ar) is accelerated to the target materials and physically demounts the target atoms, and these atoms are deposited on the substrate. The magnetron sputtering is a system in which magnets are added to the sputtering gun and improves the degree of gas ionization and the quality of the deposited thin film. The quality of the deposited thin film is affected by various factors such as base pressure, working pressure, substrate temperature, type of gas, distance between target and substrate and deposition power.

When the atmosphere inside the chamber is made into a mixed state of Ar and O_2 and target materials are deposited, the deposited atoms react with oxygen and are deposited in an oxidized state. This is called reactive sputtering. Also, the method of depositing multiple targets simultaneously in a single layer is called co-sputtering. In this thesis, we used a reactive magnetron co-sputtering method using all the methods described above as shown in Fig.13 to fabricate $\text{Co}_{0.7}\text{-Ni}_{0.3}\text{-O-Pt}$ phase alloy single layer.

The degree of vacuum inside the chamber before deposition was high vacuum with low 10^{-7} Torr and the working pressure was set to 2mTorr. The atmosphere inside the chamber is a state where Ar and O_2 gas are mixed, and the ratio of O_2 gas is adjusted to control the oxidation degree of the thin film. $\text{Co}_{0.7}\text{Ni}_{0.3}$ alloy and Pt targets which is fixed to the sputtering gun were used simultaneously so that the two materials were deposited on the single layer. At the same time, the sample stage of the chamber was rotated at a speed of 11.11rpm (5.4s/cycle) to produce a thin film. $\text{Co}_{0.7}\text{Ni}_{0.3}$ reacted with oxygen and a part of the

deposited atoms was oxidized. But Pt was deposited in a pure metal state because it is a material with low reactivity with oxygen. After depositing $\text{Co}_{0.7}\text{-Ni}_{0.3}\text{-O-Pt}$ phase alloy single layer, SiO_2 3nm was deposited to prevent native oxidation in air. In the case of the substrate, a Si (100) with SiO_2 200nm substrate was used to prevent leakage of current through the substrate.

In addition to $\text{Co}_{0.7}\text{-Ni}_{0.3}\text{-O-Pt}$, Fe-O-Pt and $\text{Co}_{0.7}\text{-Ni}_{0.3}\text{-O-Au}$ phase alloys were also fabricated in the same way to confirm the effect of AFM and spin Hall effect, respectively.

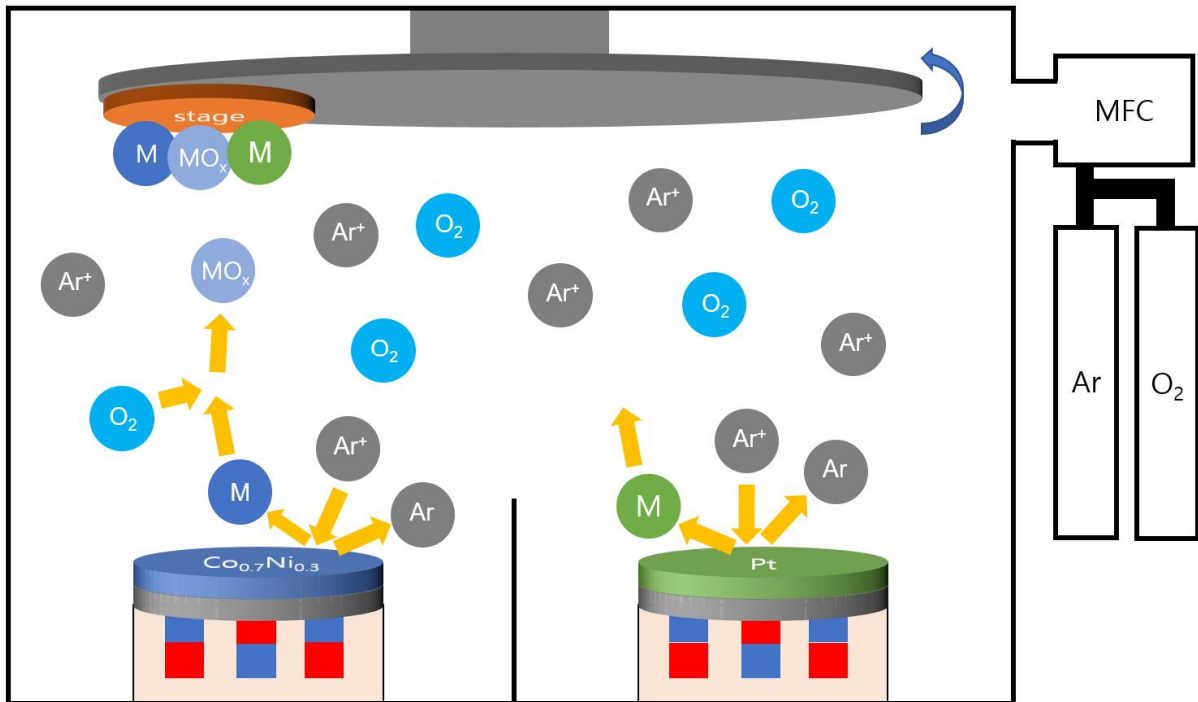


Fig. 13 Schematic of reactive magnetron co-sputtering using $\text{Co}_{0.7}\text{Ni}_{0.3}$ and Pt target for fabricating the $\text{Co}_{0.7}\text{-Ni}_{0.3}\text{-O-Pt}$ phase alloy single layer

3.1.3 Photolithography

For high current density (over 10^{10} A/m²) experiment, a Hall bar and 4probe pattern with a thickness of 10 μ m and a length of 40 μ m of one leg was fabricated through photolithography.

Photolithography is one of the useful techniques for making a sample into a micro-sized desired shape. The Photolithography process is represented in Fig.14. First, organic and inorganic impurities were removed using acetone and ethanol as the substrate. The substrate was coated with photoresist (AZ GXR-601 14CP) by a spin coater. At this time, positive photoresist was used and the rotation speed and time were 8000rpm and 60s, respectively. After the spin coating was completed, a soft bake was performed at 100°C for 60s to remove the residual solvent and dry the photoresist. The soft bake completed sample was contacted with mask which have Hall bar and 4probe pattern and exposed to ultraviolet (UV) light for 8s. The substrate after the exposure process was developed for 60s and was cleaned in DI water for 60s to remove residual developer. Due to the property of the positive photoresist used, the photoresist in the UV exposed area was removed. After depositing Co_{0.7}-Ni_{0.3}-O-Pt phase alloy single layer, it was lifted off using ultra sonication for several seconds to remove the photoresist and the thin film deposited on it.

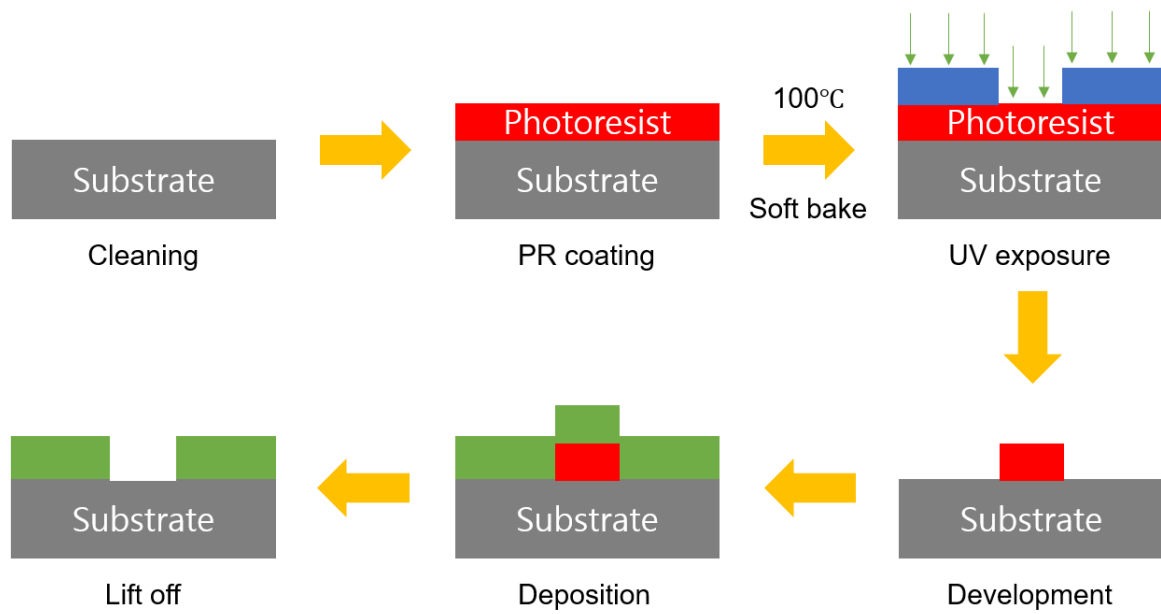


Fig. 14 Process of photolithography for fabricating patterned thin film.

3.2 structural property measurement

3.2.1 X-ray Diffraction

X-ray diffraction (XRD) is a one of the most widely used method for characterizing the crystal structure and chemical composition. Crystal refers to the regular arrangement of atoms and X-ray can be regarded as electromagnetic waves. Atoms scatter x-ray waves through electrons, and x-rays scattered by electrons produce secondary circular waves from electrons. This phenomenon is known as elastic scattering. These waves are canceled through destructive interference in most direction. However, when the following specific conditions are satisfied, constructive interference occurs and the crystal structure can be analyzed by detecting it. This condition is called Bragg's law,

$$2d \sin \theta = n\lambda$$

Where d is the spacing between the planes (d-spacing), θ is the angle between planes and the incident x-ray beam, λ is the wavelength of x-ray and n is integer representing the order of the diffraction peak.

In this thesis, crystal structure of $\text{Co}_{0.7}\text{-Ni}_{0.3}\text{-O-Pt}$ phase alloy single layers were investigated by Empyrean x-ray diffractometer (Panalytical) equipped with a Empyrean Cu LFF HR X-ray tube (Panalytical). And the type of X-ray source is Cu and use $K\alpha$ x-ray ($\lambda = 1.51487\text{\AA}$).

3.2.2 Transmission electron microscopy (TEM)

Transmission electron microscopy is a microscopic technique in which an image is formed by the interaction between electrons and the atoms in the sample as an electron beam passes through it. In the case of TEM, since the electron wavelength is smaller, an image with high resolution can be obtained compared to light microscopy. Because it uses electron beam, unlike light microscopy, images appear in contrast, but it has the advantage of being able to see the array of atoms. In addition, it is possible to map the distribution of atoms by using different interactions between the incident electron beam and the atoms depending on the element.

We measured the crystal structure of $\text{Co}_{0.7}\text{-Ni}_{0.3}\text{-O-Pt}$ phase alloy single layers depending on the degree of oxidation using TEM to confirm the more detailed nanocrystal structure. And compared with XRD data. Also, distribution of each atom was confirmed through atomic mapping.

3.2.3 Scanning Electron Microscope (SEM)

Scanning Electron Microscope is one of the equipment that measures the surface shape and elements by detecting secondary electrons, backscattered electrons and X-rays that occur when high energy electrons collide with the sample. Scanning electron Microscope-Energy Dispersive X-ray spectrometer (SEM-EDS) is a technique that can quantitatively analyze the amount of atom constituting a sample using SEM. It is measured through characteristic X-rays generated by collision between incident electron and atoms.

To confirm the atomic ratio of Co, Ni and Pt depending on degree of oxidation, SEM-EDS was performed. In addition, the atomic percent of the $\text{Co}_{0.7}\text{-Ni}_{0.3}\text{-O-Au}$ and Fe-O-Pt phase alloys prepared for comparison were also measured. Measurement conditions are 15kV acceleration voltage and $10\mu\text{A}$ current with 15mm working distance. Each film was measured for 60s at three locations. In the cases of $\text{Co}_{0.7}\text{-Ni}_{0.3}\text{-O-Au}$ and Fe-O-Pt films, atomic percent of Au and Pt was also measured with same technique.

3.3 magnetic property measurement

3.3.1 Vibrating Sample Magnetometer (VSM)

Vibrating sample magnetometer (VSM) is a conventional method for measuring magnetic properties of the magnetic materials. When the sample located between the electromagnets is vibrated in the z-axis direction, the magnetic moment of sample can be measured through the voltage induced in the pickup coils. Since the voltage induced in pickup coils does not depend on the external magnetic field, it has the advantage that only the magnetic moment of the sample can be measured. By sweeping the external magnetic field during vibrating the sample, a hysteresis loop can be obtained. And through it, it is possible to obtain the various magnetic properties of sample such as saturation magnetization (M_s), remanent magnetization (M_r), coercivity (H_c) and magnitude of exchange bias (H_E).

3.3.2 Magneto-Optical Kerr Effect microscopy (MOKE)

Magneto-Optical Kerr Effect microscopy (MOKE) is a equipment that measures the magnetic properties of a sample through changes in light reflected from magnetized surface. It is similar with the Faraday effect in terms of measuring through changes in light, but unlike the Faraday effect, which uses transmitted light, it measures the light reflected from the surface. Depending on the purpose of measurement such as out-of-plane and in-plane, it is divided into polar, longitudinal and transverse methods as shown in Fig.15.

Unlike VSM, which measures the magnetic moment of the entire film, MOKE can measure the magnetic properties of the micro-size region. It is effective in measuring the micro size pattern region made for high current density experiments. Kerr signal is affected by magnetic moment, but it has the disadvantage that quantitative value of moment cannot be obtained

To obtain changed magnetic properties caused by spin Hall effect of $\text{Co}_{0.7}\text{-Ni}_{0.3}\text{-O-Pt}$ phase alloy single layer, we measure the hysteresis loop during applying current for 5s. Also longitudinal method was used because $\text{Co}_{0.7}\text{-Ni}_{0.3}\text{-O-Pt}$ phase alloy has in-plane anisotropy. The direction of applied current, external magnetic field and hysteresis loop measurement region are shown in Fig.16.

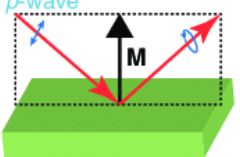
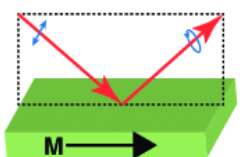
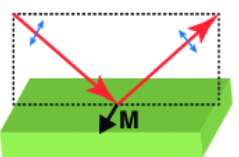
Name	(a) Polar	(b) Longitudinal	(c) Transverse
Geometry			
Detection	Out-of-plane	in-plane	in-plane
Polarization Variation	Rotation Ellipticity		None
Measurement	Polarization Analysis		Intensity measurement

Fig. 15 Schematic diagram of MOKE measurement.²⁸

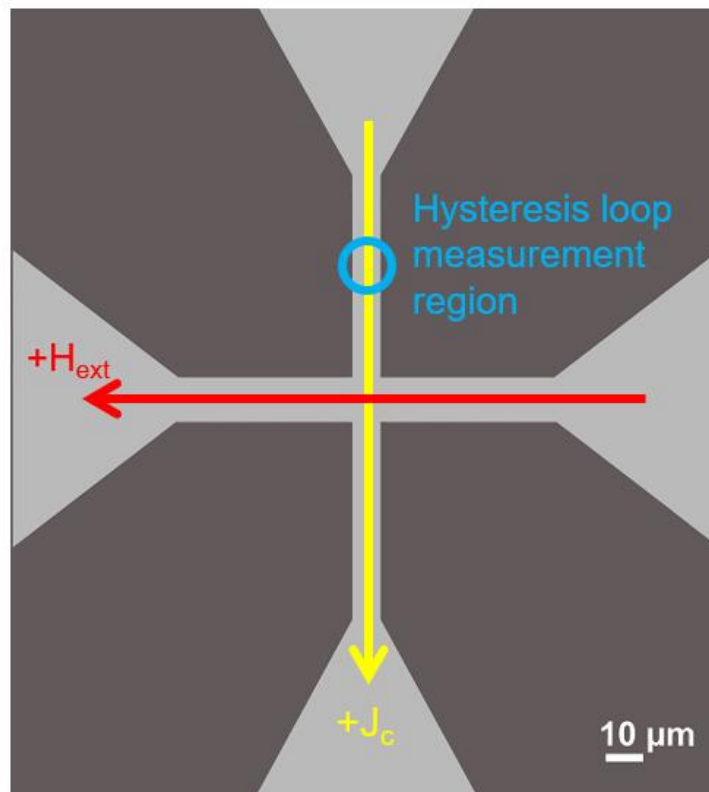


Fig. 16 Hall bar pattern for applying high current density with $10\mu\text{m}$ width and $40\mu\text{m}$ length in one leg. Direction of applied current and external magnetic field is represented by yellow and red arrow, respectively. Blue circle region is measured by MOKE.

IV. Results and Discussion

4.1 Characterization of Co_{0.7}-Ni_{0.3}-O-Pt phase alloy single layer

4.1.1 Confirm the degree of oxidation

Co_{0.7}-Ni_{0.3}-O-Pt phase alloy single layer deposited by controlling the oxygen flow rate inside the chamber has FM and AFM phases randomly distributed in one layer. Unlike Pt atoms deposited as a pure metal phase due to its low reactivity with oxygen, a part of Co_{0.7}Ni_{0.3} were deposited as metal oxide phases. The proportion of oxidized Co_{0.7}Ni_{0.3} was controlled by adjusting oxygen flow rate. And for quantitative comparison, magnetization was measured and compared through VSM.

Co_{0.7}Ni_{0.3}O is an AFM material and its net magnetic moment is close to zero. Also, since Pt is a paramagnetic material and has a disordered spin structure, the magnetic moment is very small compared to the ferromagnet. Therefore, magnitude of magnetization of these two phases can be negligible compared to that of ferromagnet. It means that the magnetization value of Co_{0.7}-Ni_{0.3}-O-Pt phase alloy single layer is determined by the Co_{0.7}Ni_{0.3} (FM) phases. Using this, a pure metal Co_{0.7}-Ni_{0.3}-Pt phase alloy single layer fabricated in an Ar atmosphere was basis as 0% oxidation degree sample, and oxidation degree of other films was confirmed according to the ratio of the magnetization value. As a result, it was confirmed that oxidation degree increased gradually from 0% to 100% oxidation with increasing oxygen flow rate. The oxygen flow rate, magnitude of magnetization and degree of oxidation of the fabricated films are shown in Table.3. Likewise, the oxidation

degree of $\text{Co}_{0.7}\text{-Ni}_{0.3}\text{-O-Au}$ and Fe-O-Pt prepared for comparison of results was confirmed in the same way.

Oxygen flow rate (sccm)	Saturation Magnetization (emu/cc)	Oxidation degree (%)
0	840	0
0.60	460	46
0.65	380	55
0.70	270	68
0.72	200	76
0.74	150	82
0.76	90	89
0.78	60	93
0.80	30	96
0.82	0	100

Table. 3 Magnitude of saturation magnetization and oxidation degree of $\text{Co}_{0.7}\text{-Ni}_{0.3}\text{-O-Pt}$ phase alloy single layer depending on oxygen flow rate.

4.1.2 Crystal structure of $\text{Co}_{0.7}\text{-Ni}_{0.3}\text{-O-Pt}$ depending on degree of oxidation

For analyzing the crystal structure of phase alloy single layer films, X-ray diffraction (XRD) was performed. First, Pt and Au single layer films were deposited at a higher oxygen flow rate and then measured by XRD to confirm that the Pt and Au atoms were deposited in a pure metal state without oxidation. As a result, it was confirmed that Pt and Au films were grown to pure metal in an environment with a higher oxygen flow rate (0.9sccm) than the condition in which phase alloy single layer films were completed oxidized (0.82). It is shown in Fig. 17 (a) and Fig. 17 (b).

As shown in the result of $\text{Co}_{0.7}\text{-Ni}_{0.3}\text{-Pt}$ (0% oxidation degree), only $\text{Co}_{0.7}\text{-Ni}_{0.3}\text{-Pt}$, not the separated peak such as $\text{Co}_{0.7}\text{Ni}_{0.3}$ and Pt, peak appeared. It means that film was grown as alloy, not compound.

With decreasing saturation magnetization, $\text{Co}_{0.7}\text{Ni}_{0.3}\text{O}$ (111) peak appeared above 68% oxidation degree and it indicates that $\text{Co}_{0.7}\text{Ni}_{0.3}$ (FM) was oxidized and became $\text{Co}_{0.7}\text{Ni}_{0.3}\text{O}$ (AFM) as mentioned above. It leads to shift of peak position of $\text{Co}_{0.7}\text{-Ni}_{0.3}\text{-Pt}$ (111) plane.

As shown in Fig. 18 (a), the XRD peak position of $\text{Co}_{0.7}\text{Ni}_{0.3}\text{Pt}$ (111) shifted to low angle from 42.2 to 40.5 as the function of oxidation degree. A shift of XRD peak position to low angle is caused by change of atomic ratio of Pt in $\text{Co}_{0.7}\text{-Ni}_{0.3}\text{-Pt}$ phase. With the increase of the oxidation degree, the $\text{Co}_{0.7}\text{Ni}_{0.3}\text{O}$ phases were formed. Therefore, the $\text{Co}_{0.7}\text{Ni}_{0.3}$ ratio inside the $\text{Co}_{0.7}\text{-Ni}_{0.3}\text{-Pt}$ phase decrease and the Pt ratio increase. Due to this, the peak position of the $\text{Co}_{0.7}\text{-Ni}_{0.3}\text{-Pt}$ metallic phase was shifted in the direction of Pt (111) plane peak, it can be interpreted by Vegard's law. It also appears as a change in d-spacing. The d-spacing of the $\text{Co}_{0.7}\text{-Ni}_{0.3}\text{-Pt}$ (111) plane increased form 0.21nm to 0.23nm. Because the atomic size

of Pt is larger than Co and Ni. D-spacing was calculated according to Bragg's law.

$$\text{Bragg's law : } 2d \sin \theta = n\lambda$$

Where d is the spacing between the planes (d-spacing), θ is the angle between planes and the incident beam and λ is the wavelength of x-ray.

In addition, the points are decrease of peak intensity and increase of peak width of $\text{Co}_{0.7}\text{-Ni}_{0.3}\text{-Pt}$ (111) plane. These two factors are strongly affected by crystallinity. So it leads to the decline of crystallinity.

For quantitative analysis, we calculated the crystallite size from FWHM of $\text{Co}_{0.7}\text{-Ni}_{0.3}\text{-Pt}$ (111) plane peak through Scherrer equation. As shown in Fig. 19, with increase of oxidation degree, FWHM of peak is increased and crystallite size is decreased from 10nm to 3nm. Crystallite size is more small or equal with grain size. In this result, we can estimate that the grain size of oxidized phase alloy single layer is formed in few nanometer-sized grains. It shows the decline of crystallinity and leads to high density of interface. Through the result, improvement of interface effect can be expected.

The atomic percent which is measured by SEM-EDS of Pt contained in all $\text{Co}_{0.7}\text{-Ni}_{0.3}\text{-O-Pt}$ films was analogous to about ~12%.

Transmission electron microscopy (TEM) was performed for analyzing the more detail nanocrystal structure of $\text{Co}_{0.7}\text{-Ni}_{0.3}\text{-O-Pt}$ films. Fig. 20 (a) and Fig. 20 (b) are cross-sectional HRTEM images of 0% and 82% oxidation degree films, respectively. In the TEM image of 0% oxidation degree, it can be seen that the grain region and the film have grown into polycrystal structure through the partial regular atomic arrangement in most regions. Although there is a low portion of non-crystalline regions, this region is interpreted as a disordered region or a grain boundary in which atoms arranged in different directions exist together.

In contrast, in the TEM image of the 82% oxidation degree $\text{Co}_{0.7}\text{-Ni}_{0.3}\text{-O-Pt}$ film, the grains were formed in few nanometer-size and the portion of regions which have disordered atomic

arrangement was dominant. These structural features are similar to those of a typical metallic amorphous alloy. In addition, grain boundary can be interpreted as interface between the phases. Through this result, the 82% oxidized sample has more interface caused by few nanometer-sized grains, it leads to improvement of interface effect. The decline of grain size and crystallinity confirmed by TEM correspond to the results of XRD data depending on oxidation degree.

Fig. 21 shows the images that map the distribution of atoms through TEM. Except for the oxygen region measured from SiO₂ used as substrate and capping layer, all atoms of Co, Ni, O and Pt are randomly distributed throughout a layer.

Therefore, we named the structure of these thin films as Co_{0.7}-Ni_{0.3}-O-Pt phase alloy single layer because each phase is randomly distributed in the form of sub-nanometer sized grain like alloy. Also, it was expected that the spin structure could be effectively controlled by spin torque caused by spin Hall effect due to the increase of interface between each phase coming from few nanometer-sized grains.

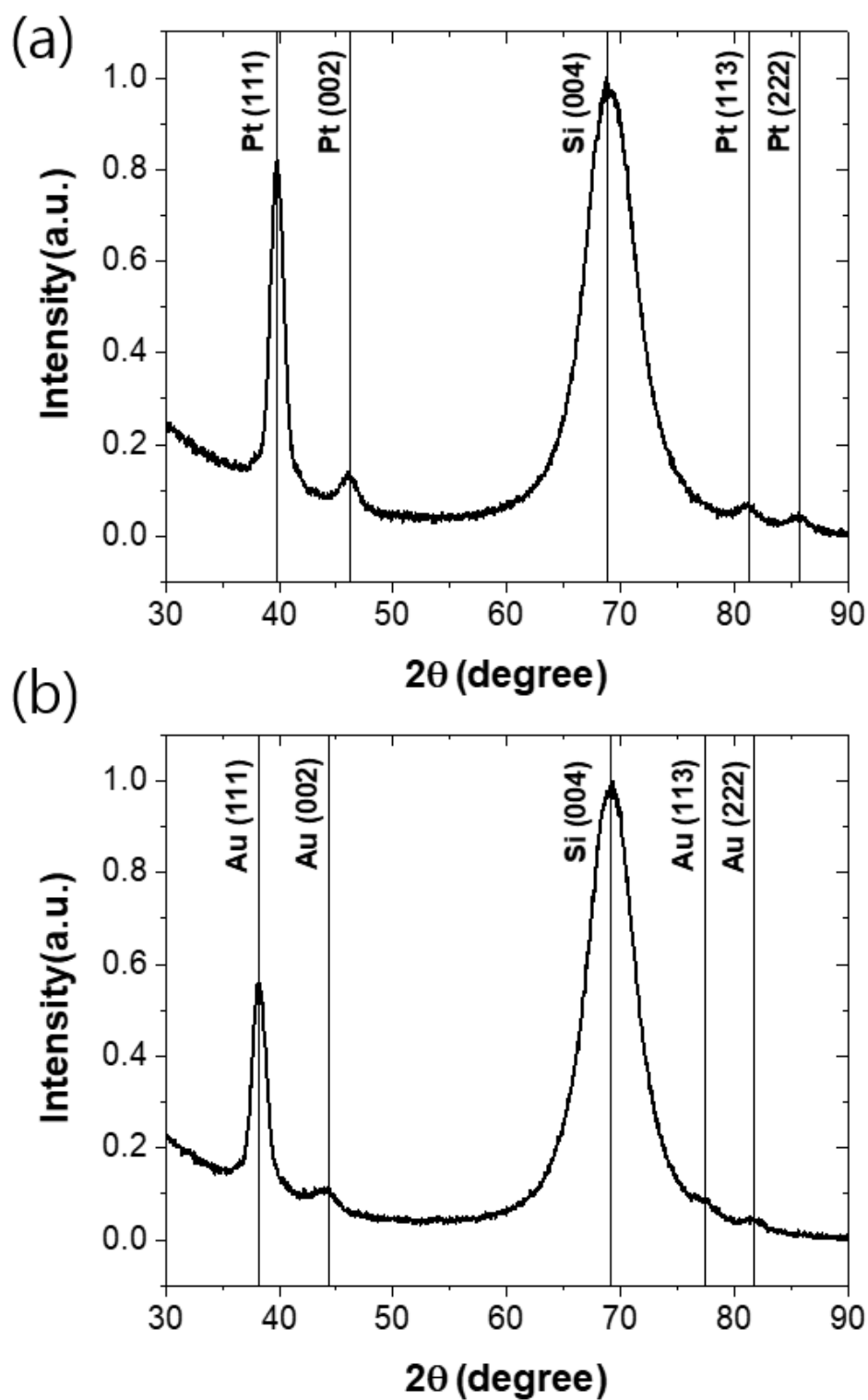


Fig. 17 XRD patterns of (a) Pt and (b) Au film deposited in Ar + O₂ (0.9sccm) atmosphere.

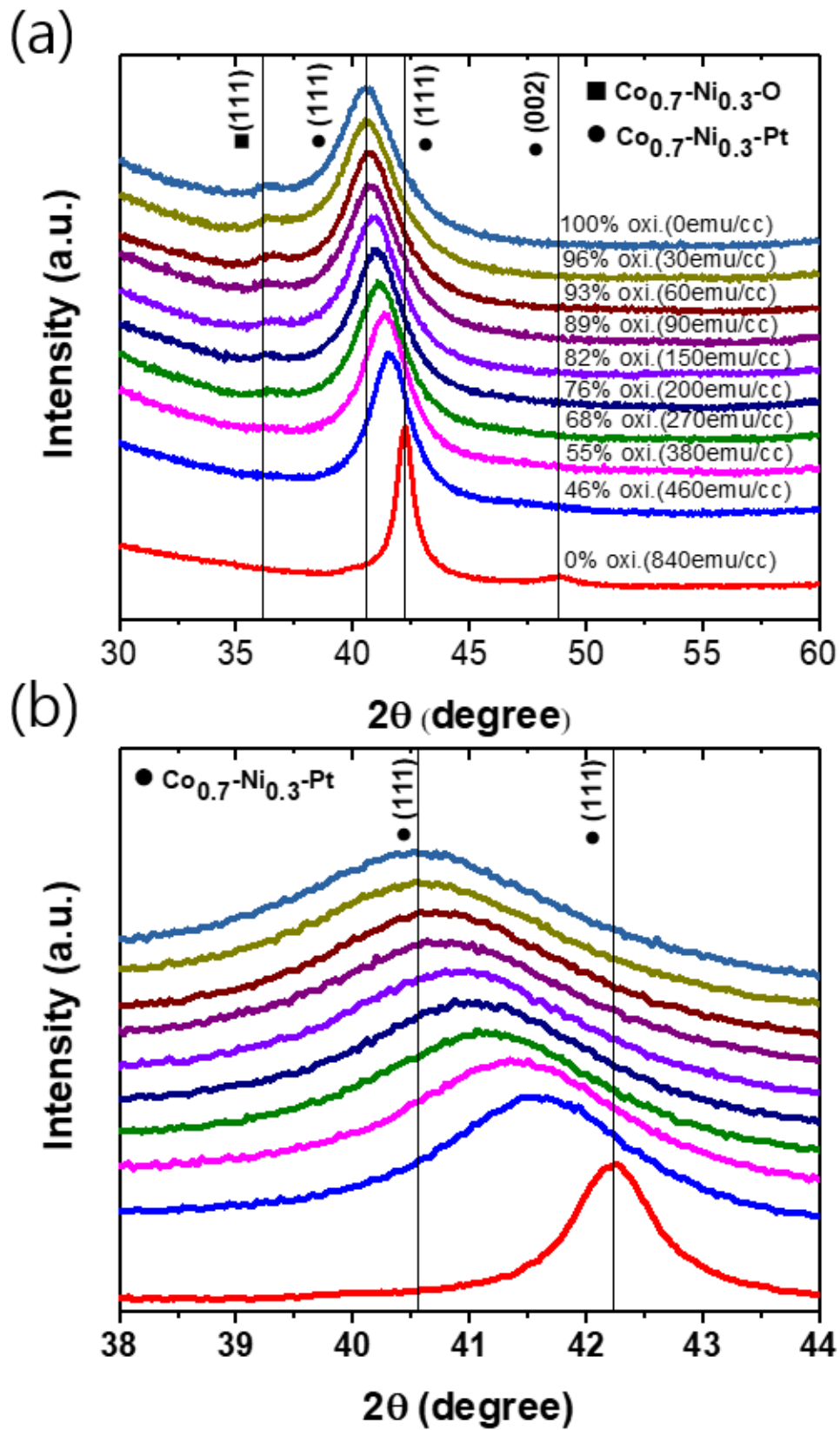


Fig. 18 (a) XRD patterns of $\text{Co}_{0.7}\text{-Ni}_{0.3}\text{-O-Pt}$ phase alloy single layers depending on oxidation degree and (b) enlarged XRD pattern to confirm the decline of crystallinity

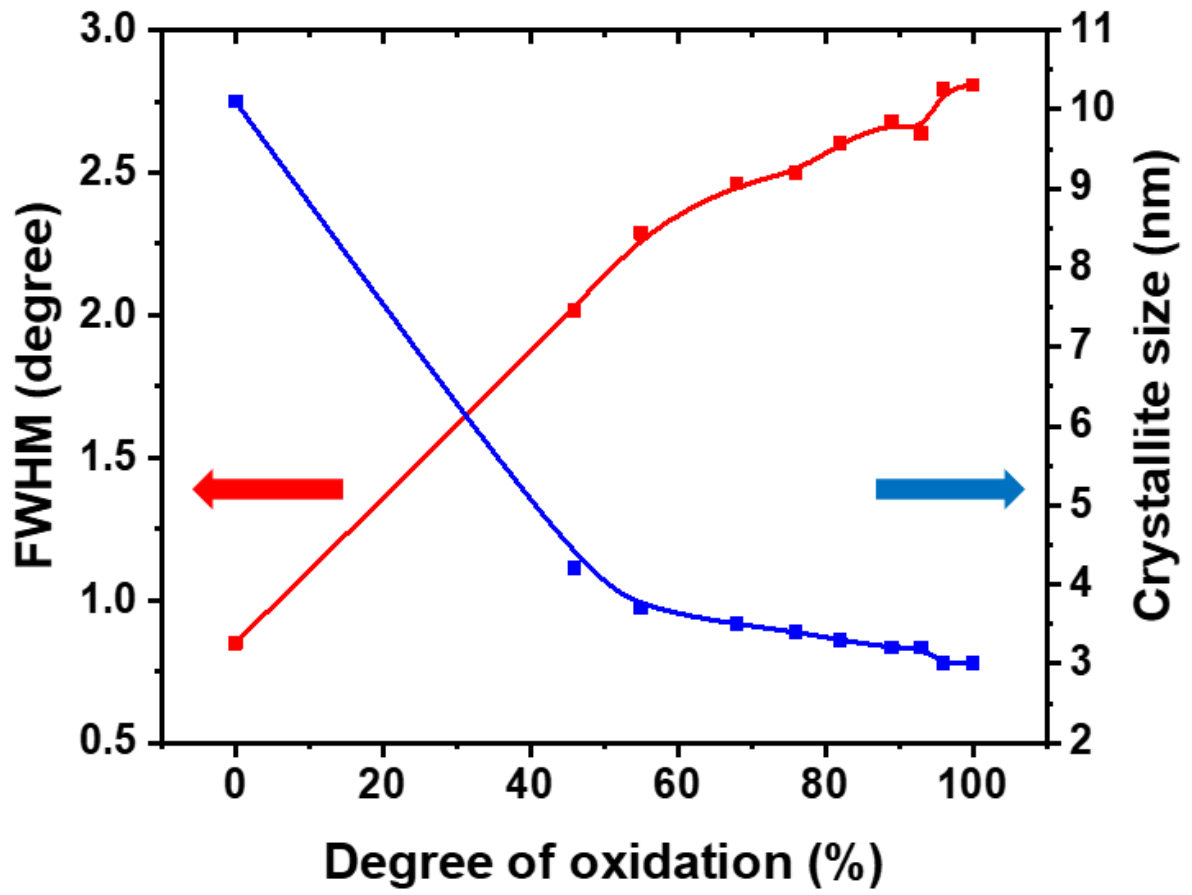


Fig. 19 FWHM (full width half maximum) of $\text{Co}_{0.7}\text{-Ni}_{0.3}\text{-O-Pt}$ (111) peak and crystallite size depending on oxidation degree

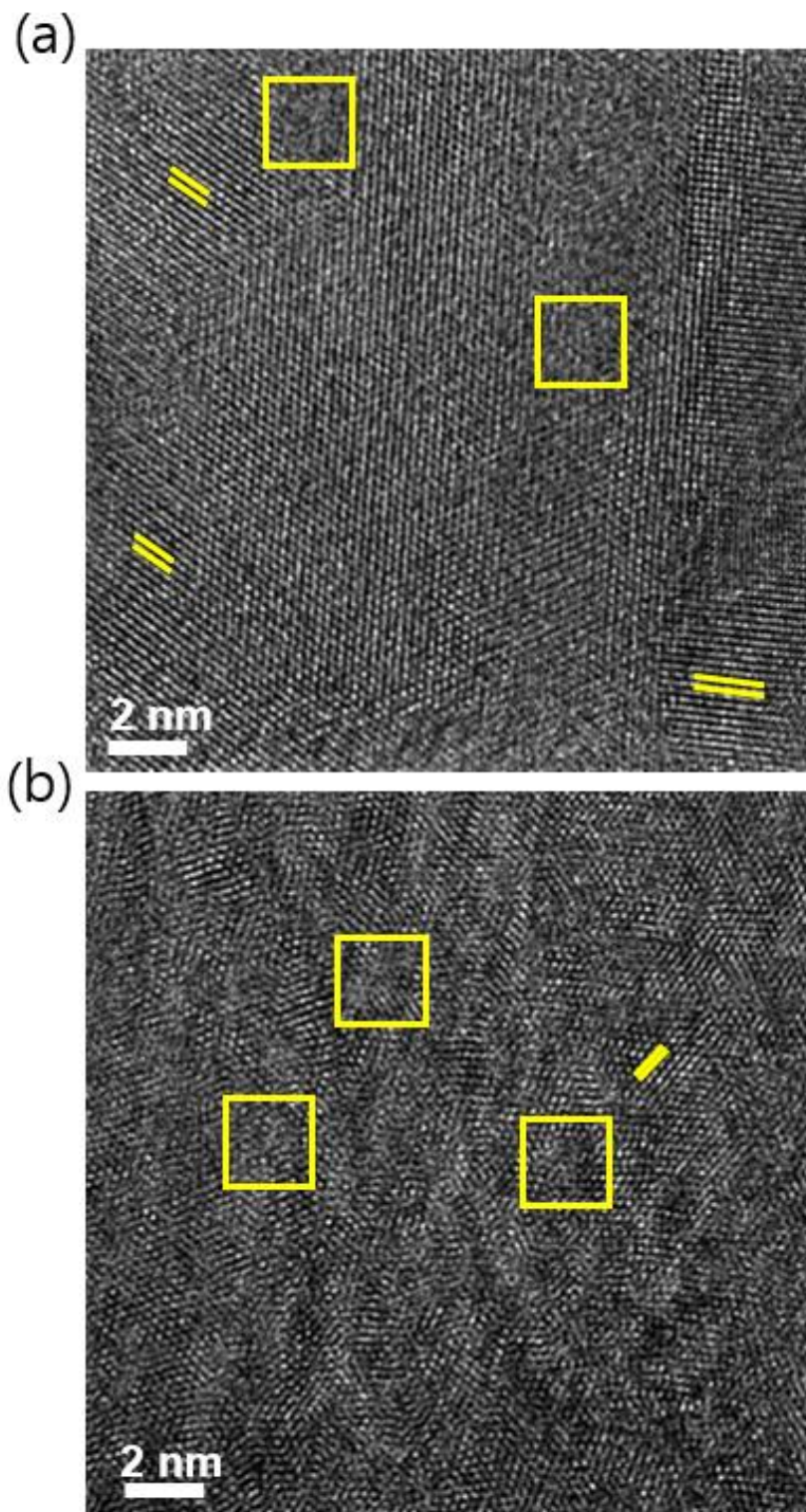


Fig. 20 TEM image of (a) 0% oxidation degree and (b) oxidation degree of $\text{Co}_{0.7}\text{-Ni}_{0.3}\text{-O-Pt}$ films. Yellow line and rectangle represent the crystalline and grain boundary, respectively.

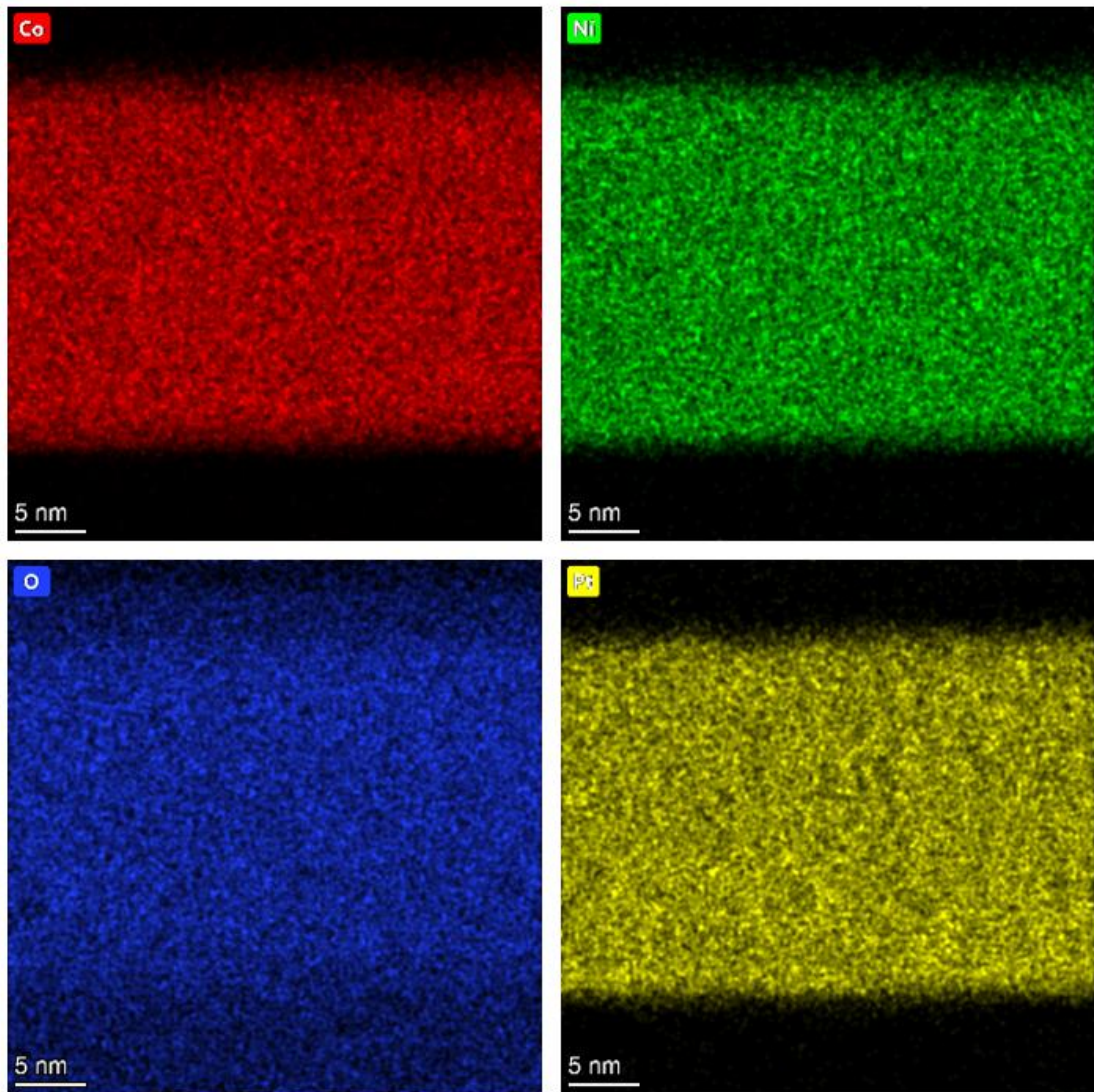


Fig. 21 Atomic mapping image measured by TEM of 82% oxidation degree $\text{Co}_{0.7}\text{-Ni}_{0.3}\text{-O-Pt}$ phase alloy single layer.

4.2 Controlled magnetic properties by spin Hall effect

4.2.1 Aligned AFM and interface effect through spin Hall effect

Polarized spins caused by the current flowing heavy-metal layer which have large spin-orbit coupling are split to opposite direction from each other. The neighboring magnetic layers can be affected and spins of magnetic layers can be rotated by polarized spins, which is called 'spin torque'. Unlike the reported layered structure, we attempt to manipulate spin structure with $\text{Co}_{0.7}\text{-Ni}_{0.3}\text{-O-Pt}$ phase alloy single layer by spin torque through spin Hall effect (SHE). In order to identify the affected spin structure of phase alloy by spin torque, hysteresis loops were measured by MOKE during applying current for 5 seconds.

In order to confirm the aligned Neel axis of AFM by spin torque caused by spin Hall effect, we prepared the phase alloy films such as a) $\text{Co}_{0.7}\text{-Ni}_{0.3}\text{-Pt}$, b) 82% oxidation degree $\text{Co}_{0.3}\text{-Ni}_{0.3}\text{-O-Pt}$, c) 78% oxidation degree $\text{Co}_{0.7}\text{-Ni}_{0.3}\text{-O-Au}$ and d) 79% oxidation degree Fe-O-Pt .

As a result of measuring the hysteresis loops of $\text{Co}_{0.7}\text{-Ni}_{0.3}\text{-Pt}$ (0% oxidation degree), no changes of hysteresis loops were observed at $J_c=1 \times 10^{11} \text{A/m}^2$ compared to the initial hysteresis loop. It has been already reported in the FM/HM structure experiment that the spin structure of FM layer can be affected and rotated by spin torque caused by spin Hall effect. It is interpreted that spin-torques affecting to spins of FM phases were canceled out by the randomly distributed Pt. In addition, it is considered that the oersted field induced by the current which flows phase alloy layer is also canceled inside the layer.

On the other hand, the exchange bias breaking symmetry of hysteresis loop was induced in the 82% oxidation degree of $\text{Co}_{0.7}\text{-Ni}_{0.3}\text{-O-Pt}$ phase alloy film at $J_c= 4.62 \times 10^{11} \text{A/m}^2$ as shown

in Fig. 22 (b). By comparing the hysteresis loop when current flows and doesn't flow through film, it can be interpreted that the Neel axis of the AFM is aligned by spin torque and aligned spins of AFM coupled with spins of FM during applying current at the interface between FM and AFM phases.

To confirm that the induced exchange bias was caused by SHE, we prepared 78% oxidation degree of $\text{Co}_{0.7}\text{-Ni}_{0.3}\text{-O-Au}$ phase alloy film. As a well-known fact, the spin Hall angle of Au is smaller than Pt, so magnitude of spin current generated by spin Hall effect is also weak. Also, the resistivity of Au and Pt is $2.44 \times 10^{-8} \Omega\cdot\text{m}$ and $1.06 \times 10^{-7} \Omega\cdot\text{m}$, respectively. The atomic percent of Au contained in the $\text{Co}_{0.7}\text{-Ni}_{0.3}\text{-O-Au}$ films was identified by SEM-EDS, about ~14%, similar to that of $\text{Co}_{0.7}\text{-Ni}_{0.3}\text{-O-Pt}$ films. Therefore, when a current is applied to films, magnitude of current flowing through the heavy metal phases is larger in $\text{Co}_{0.7}\text{-Ni}_{0.3}\text{-O-Au}$ films than $\text{Co}_{0.7}\text{-Ni}_{0.3}\text{-O-Pt}$. So it is suitable to confirm the effect of spin Hall effect and oersted field. As shown in Fig. 22 (c), the exchange bias did not appear. The decrease of coercivity when current is applied is considered due to heat. From these results, it is interpreted that the induced exchange bias of $\text{Co}_{0.7}\text{-Ni}_{0.3}\text{-O-Pt}$ film was due to the spin torque acting by the spin Hall effect, and that the oersted field was canceled out or has no effective influence.

In addition, to identify that the effect of spin structure of aligned AFM, 79% oxidation degree Fe-O-Pt film was prepared. Neel temperature of FeO is 193K, so FeO is paramagnetic in room temperature. Because of it, we can clarify whether the induced exchange bias was due to aligned AFM or not by comparing results. As shown in Fig. 22 (d), any changes do not appear.

Fig. 23 shows the magnitude of the induced exchange bias depending on applied current

density of each film. As mentioned above, exchange bias was applied only to the 82% oxidation degree $\text{Co}_{0.7}\text{-Ni}_{0.3}\text{-O-Pt}$ film, and its size was proportional to the current density. It indicates that the strength of spin torque was increased with increase of current density and align the spin structure of AFM more effectively. It is consistent with what was mentioned in section 2.6

Therefore, the induced exchange bias was caused by the exchange coupling of the interface spins between the AFM phases aligned by spin torque and FM phases.

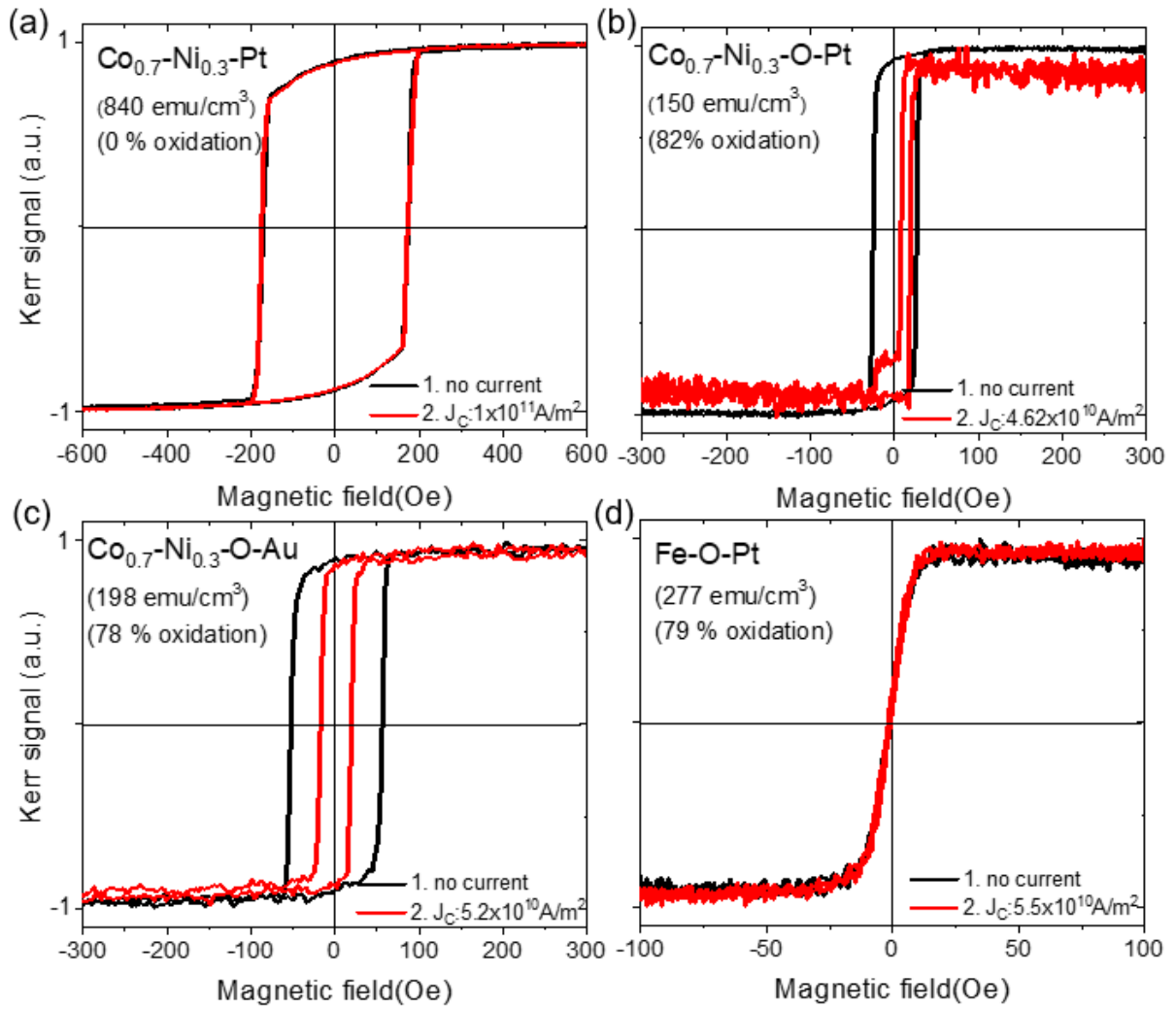


Fig. 22 Hysteresis loops measured by MOKE of (a) 0%, (b) 82% oxidation degree of $\text{Co}_{0.7}\text{-Ni}_{0.3}\text{-O-Pt}$, (c) 78% oxidation degree of $\text{Co}_{0.7}\text{-Ni}_{0.3}\text{-O-Au}$ and (d) 79% oxidation degree of Fe-O-Pt phase alloy. Black line is measured without current and red line is measured during applying current.

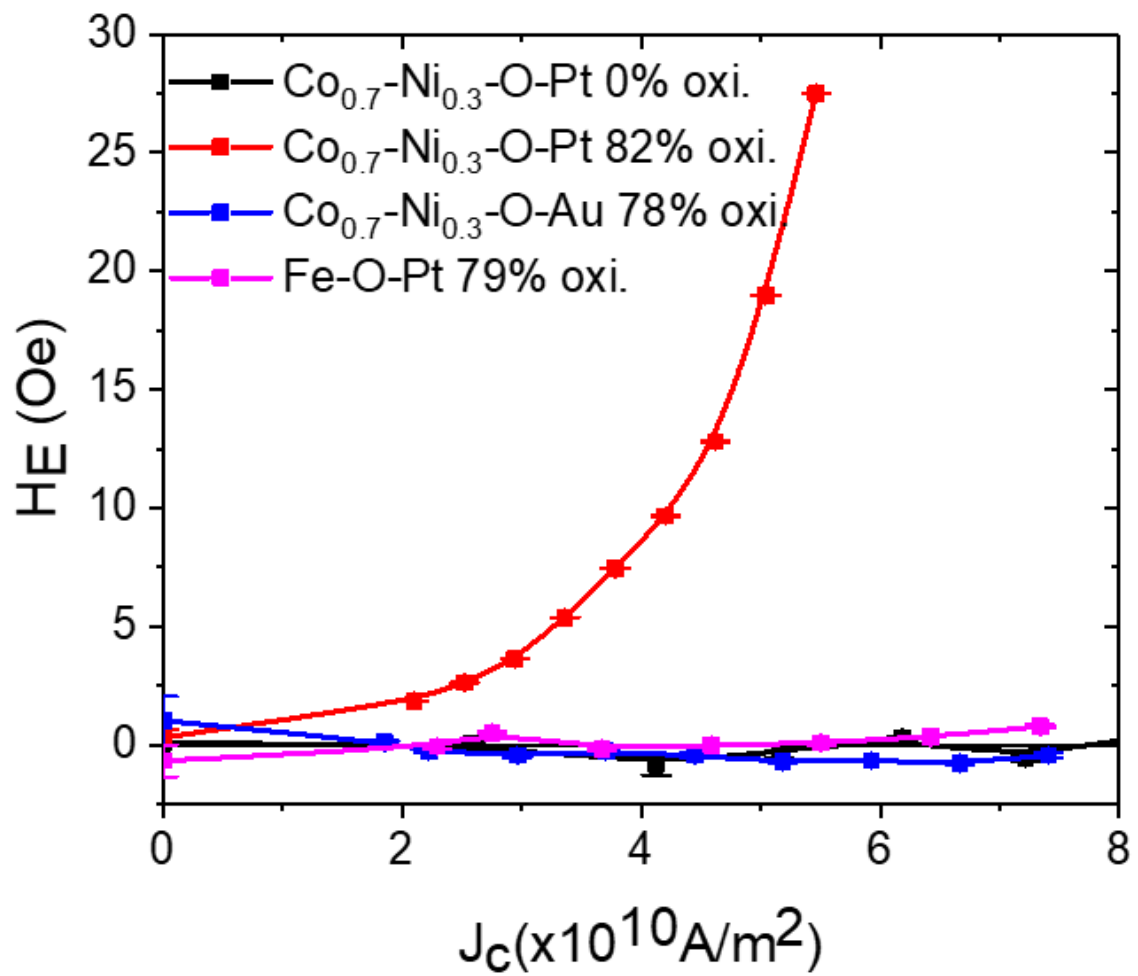


Fig. 23 Magnitude of induced exchange bias depending on current density of phase alloy single layers.

4.2.2 Magnitude of induced exchange bias depending on oxidation degree and current density

As mentioned in section 2.6, the strength of spin torque caused by spin Hall effect is proportional to the current density flowing through the heavy metal. In addition, it has already been reported that the interfacial effect of phase alloy single layer can be affected by oxidation degree of film. For this reason, we confirmed the dependence on current density and oxidation degree of films.

Induced exchange bias increases in proportion to current density and oxidation degree of films as shown in Fig. 24. This is closely related to the strength of spin torque affecting the spin structure of AFM. As the current density flowing through Pt phases increases, a larger spin Hall effect is generated, which leads to an increase in the strength of spin torque. For this reason, the induced exchange bias was proportional to the applied current density.

However, the exchange bias was not applied to all films. As shown in Fig. 24, the degree of oxidation of the films also affects the magnitude and occurrence of the exchange bias. We interpreted the cause in two ways.

The first is the increase of the insulator ratio inside the film. The strength of spin torque caused by spin Hall effect is proportional to charge current density flowing through heavy metal phase. In the $\text{Co}_{0.7}\text{-Ni}_{0.3}\text{-O-Pt}$ phase alloy single layer, as charge current density flowing through Pt phases, the strength of spin torque is reinforced. As is well known, $\text{Co}_{0.7}\text{Ni}_{0.3}\text{O}$ is an insulator material. Therefore, when the same amount of current density was applied, the higher the oxidation degree, the more current flows through Pt. Increase of oxidation degree is reflected decrease of saturation magnetization and increase of resistance

as shown in Fig.25. Another factor is the change in the interface between phases. As analyzed in section 4.1, crystallinity and grain size declined with an increase of oxidation degree. This leads to an increase of the interfacial region between each phase. It is reflected as magnitude of exchange bias caused Remarkably exchange bias was induced at $J_c \sim 10^{10} \text{ A/m}^2$, which is an order lower than reported $J_c \sim 10^{11} \text{ A/m}^2$.

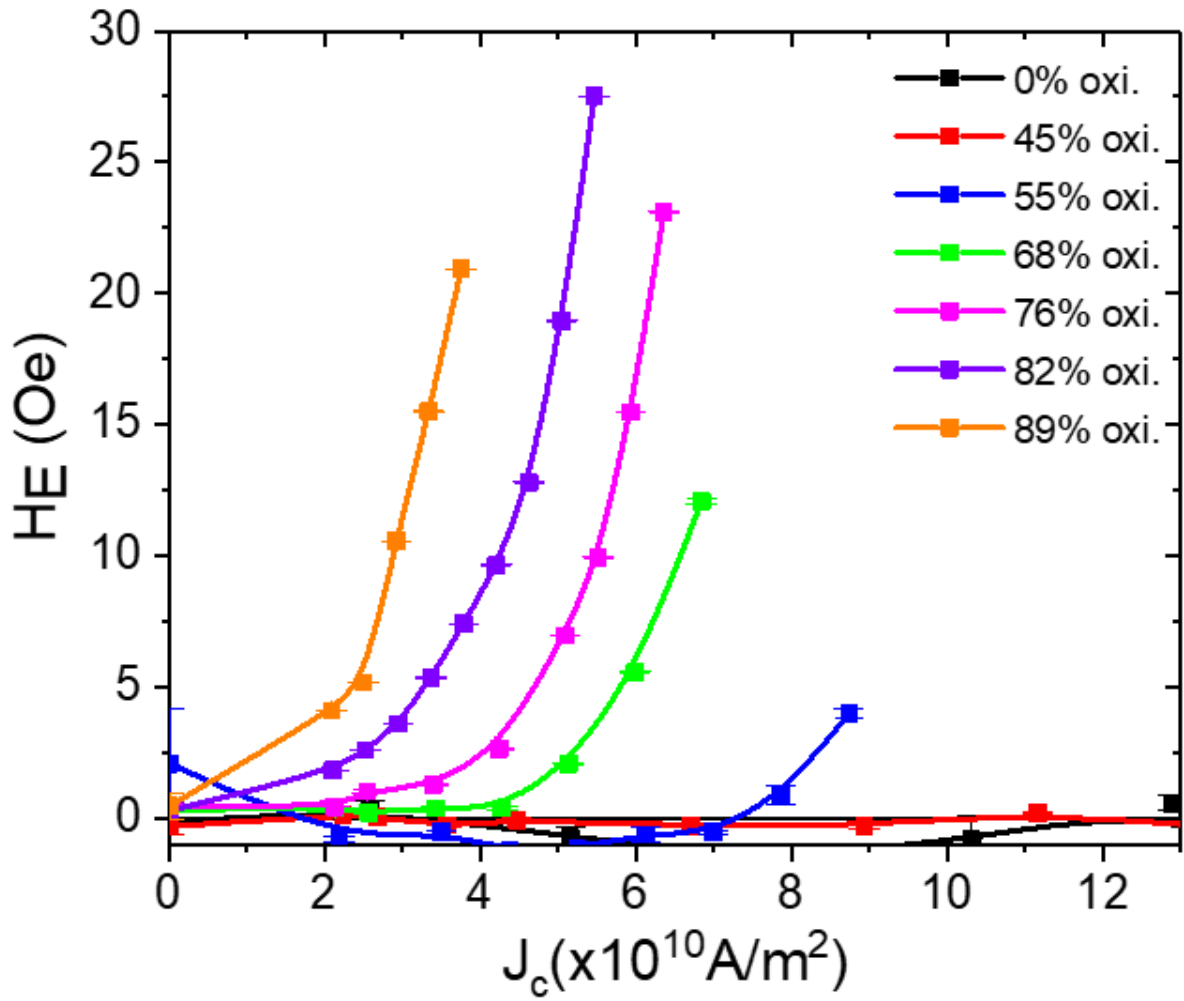


Fig. 24 Magnitude of induced exchange bias depending on current density and oxidation degree of $\text{Co}_{0.7}\text{-Ni}_{0.3}\text{-O-Pt}$ phase alloys.

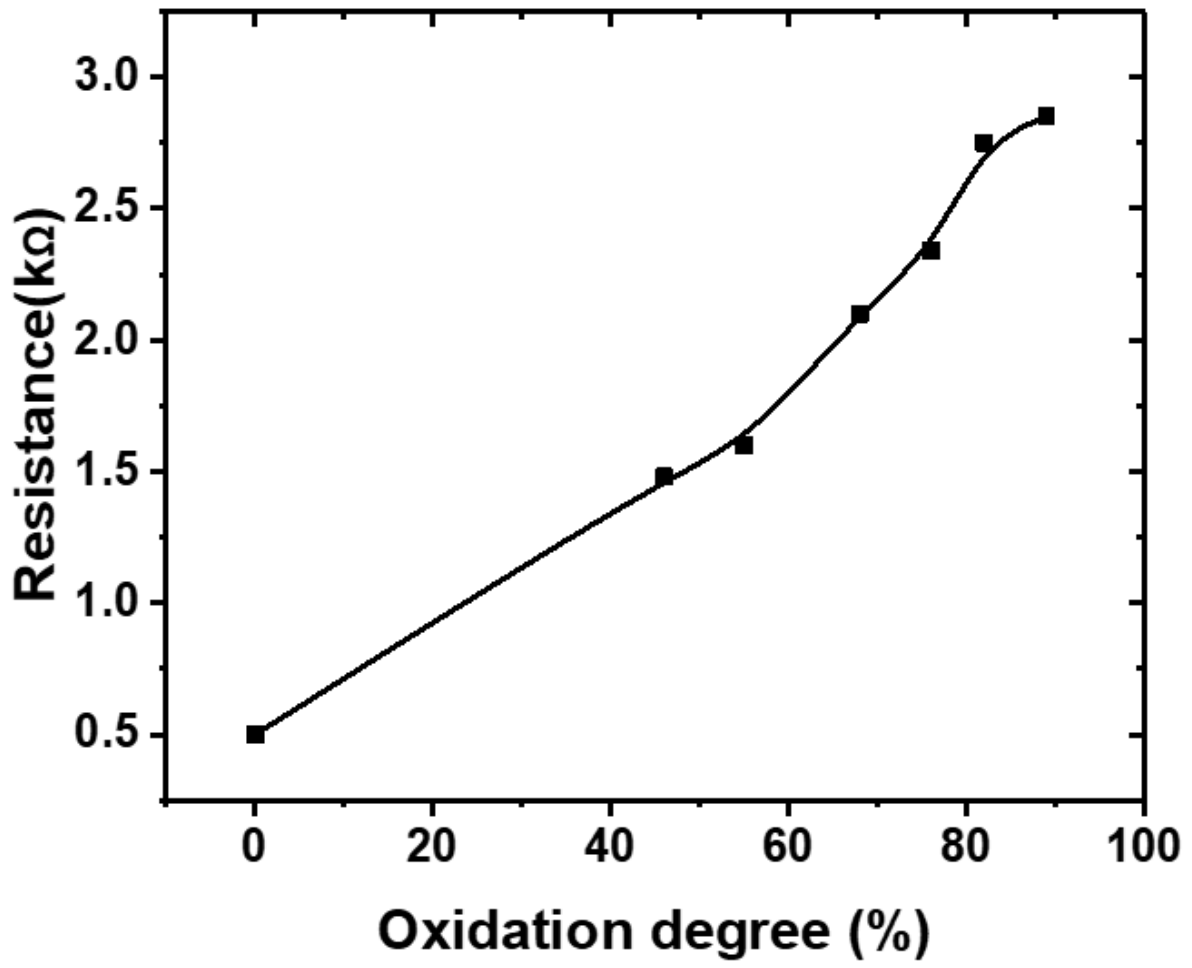


Fig. 25 Resistance of $\text{Co}_{0.7}\text{-Ni}_{0.3}\text{-O-Pt}$ phase alloy single layer depending on oxidation degree

4.2.3 Reversible and repeatable exchange bias depending on direction of charge current

In the previous section, we found that the spin structure of AFM can be controlled by the spin torque generated by the spin Hall effect at a current density that is one order lower than that reported. In this section, we applied positive and negative currents and measured each hysteresis loops to confirm the dependence of the induced exchange bias on the polarized spin direction.

As shown in Fig.26, when \pm current, $J_c = \pm 4.62 \times 10^{10} \text{A/m}^2$, was applied to 82% oxidation degree $\text{Co}_{0.7}\text{-Ni}_{0.3}\text{-O-Pt}$, exchange bias was induced in opposite directions. Also, repeatability of induced exchange bias was confirmed through the result of repeatedly applying the reversed current. (Fig. 27) In conclusion, the induced exchange bias is effectively applied and reversed by the polarized spin direction of the SHE.

In addition, the exchange bias can be reversed, which is also seen at 68% oxidation degree, in the range of current density form $-7 \times 10^{10} \text{A/m}^2$ to $+7 \times 10^{10} \text{A/m}^2$. (Fig. 28)

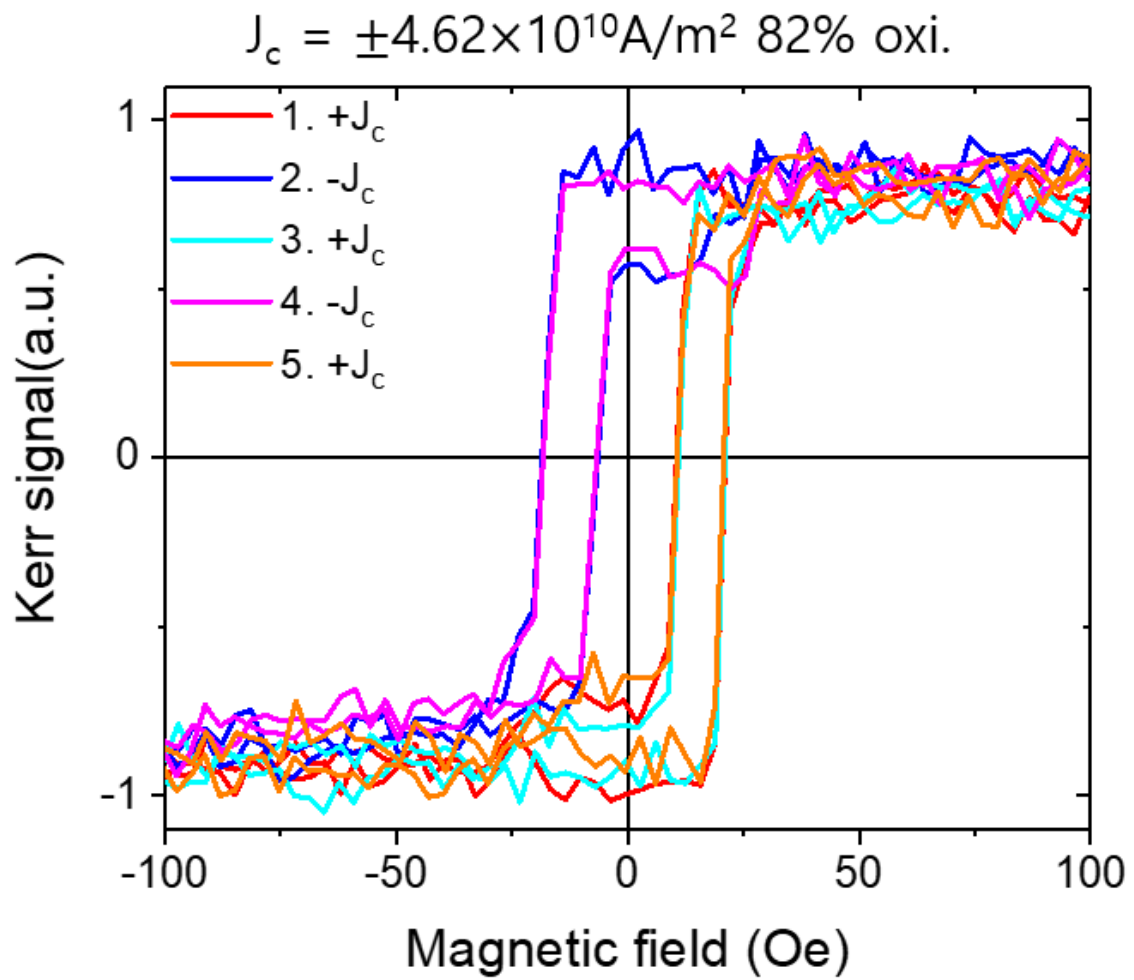


Fig. 26 Hysteresis loops of 82% oxidized $\text{Co}_{0.7}\text{-Ni}_{0.3}\text{-O-Pt}$ when $J_c = \pm 4.62 \times 10^{10} \text{ A/m}^2$ is repeatedly applied.

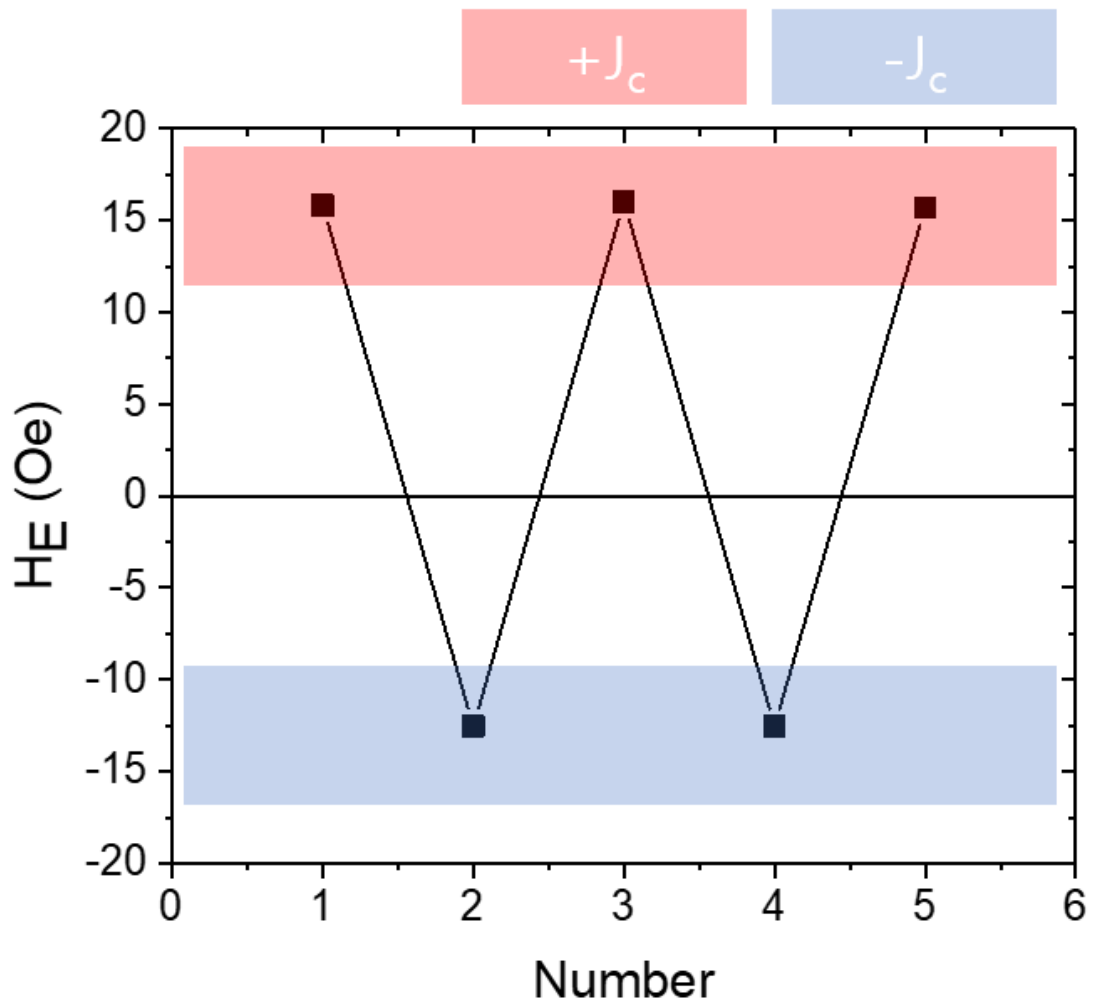


Fig. 27 Magnitude of induced exchange bias of 82% oxidized Co_{0.7}-Ni_{0.3}-O-Pt when $J_c = \pm 4.62 \times 10^{10} \text{ A/m}^2$ is repeatedly applied.

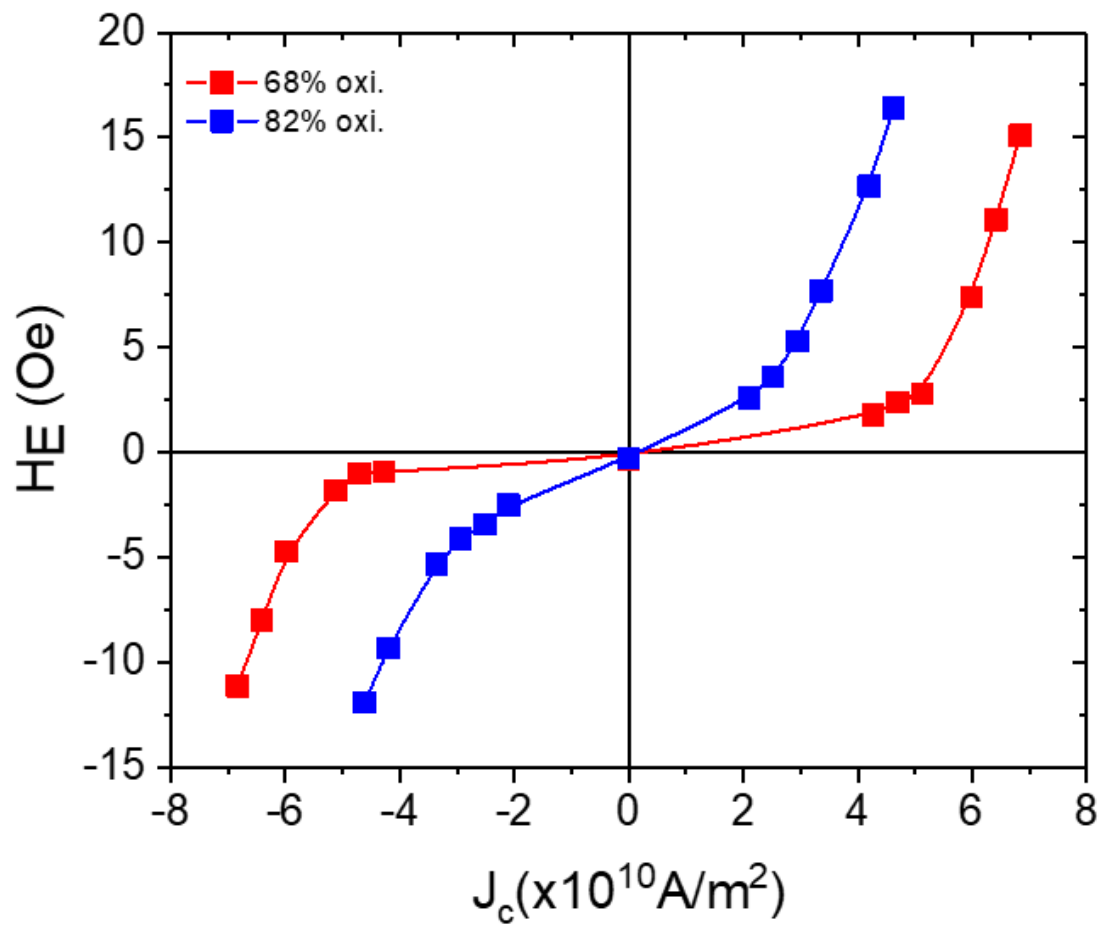


Fig. 28 Magnitude of induced exchange bias of 68% and 82% oxidized Co_{0.7}-Ni_{0.3}-O-Pt by sweeping current density.

4.2.4 Field-free magnetization switching

It is reported that the magnetization of FM and Neel axis of AFM can be switched by SHE in layered structure. In reported studies, it requires high current density, over $J_c \sim 10^{11} \text{A/m}^2$. On the other hand, as shown in Fig. 29, it was confirmed that the magnetic moment can be aligned in the same direction at external field is zero regardless the direction of sweeping field with low current density ($\sim 10^{10} \text{A/m}^2$). The direction of aligned magnetic moment depends on the applied charge current direction. When the positive current is applied, magnetic moment is aligned in negative direction. And when the negative current is applied, opposite result appears. Through this result, we think that the magnetic moment can be switched by induced exchange bias without external magnetic field. But in the case of hysteresis loop measurement, we cannot remove the effect of external field, so we measured the magnetic domain without sweeping field.

Before applying the current, the magnetic moment of the 82% oxidation sample was saturated by $\pm x$ direction to the external field, and the magnetic domain was measured by MOKE. The black region and white region of the domain image represent the magnetic moment in the $\pm x$ direction, respectively. Fig. 30 (a) and (d) are domain images when magnetic moment was saturated in the $\pm x$ direction by external field before applying current. It was shown that all regions on which the film was deposited were saturated by and external field. During applying current, $J_c = \pm 4.2 \times 10^{10} \text{A/m}^2$, changes of domain were shown in Fig. 30 (b) and (e). Unlike when saturated by external field, only the domain of the line area to which high density current is applied was switched in the opposite direction. Also, this switched direction is consistent with the magnetic moment direction controlled by the induced exchange bias at the point where the external field is 0, as shown in Fig. 29. After

current was turned off, remanence magnetization was formed in the switched direction and it was reflected by domain. (Fig.30 (c) and (f)). In the case of square area in the center of the Hall bar pattern, as shown in Fig. 30(b),(c),(e),(f), magnetization switching did not occur, but unlike the line area, it is interpreted that the high current density could not be maintained due to the line area made in the x-axis direction in the square area.

When measuring the hysteresis loops, it was difficult to exclude the dependence on the external magnetic field due to the characteristic of the method of sweeping the external magnetic field while current is applied. On the other hand, in the case of the domain measurement performed in this section, it was possible to exclude the dependence of the external field except for aligning the magnetic moment before applying the current. As a result, we show that field-free magnetization switching through SHE can be performed with low current density $J_c \sim 10^{10} \text{A/m}^2$ in $\text{Co}_{0.7}\text{-Ni}_{0.3}\text{-O-Pt}$ phase alloy single layer instead of layered structure.

$J_c = \pm 4.2 \times 10^{10} \text{ A/m}^2$ in 82% oxi.

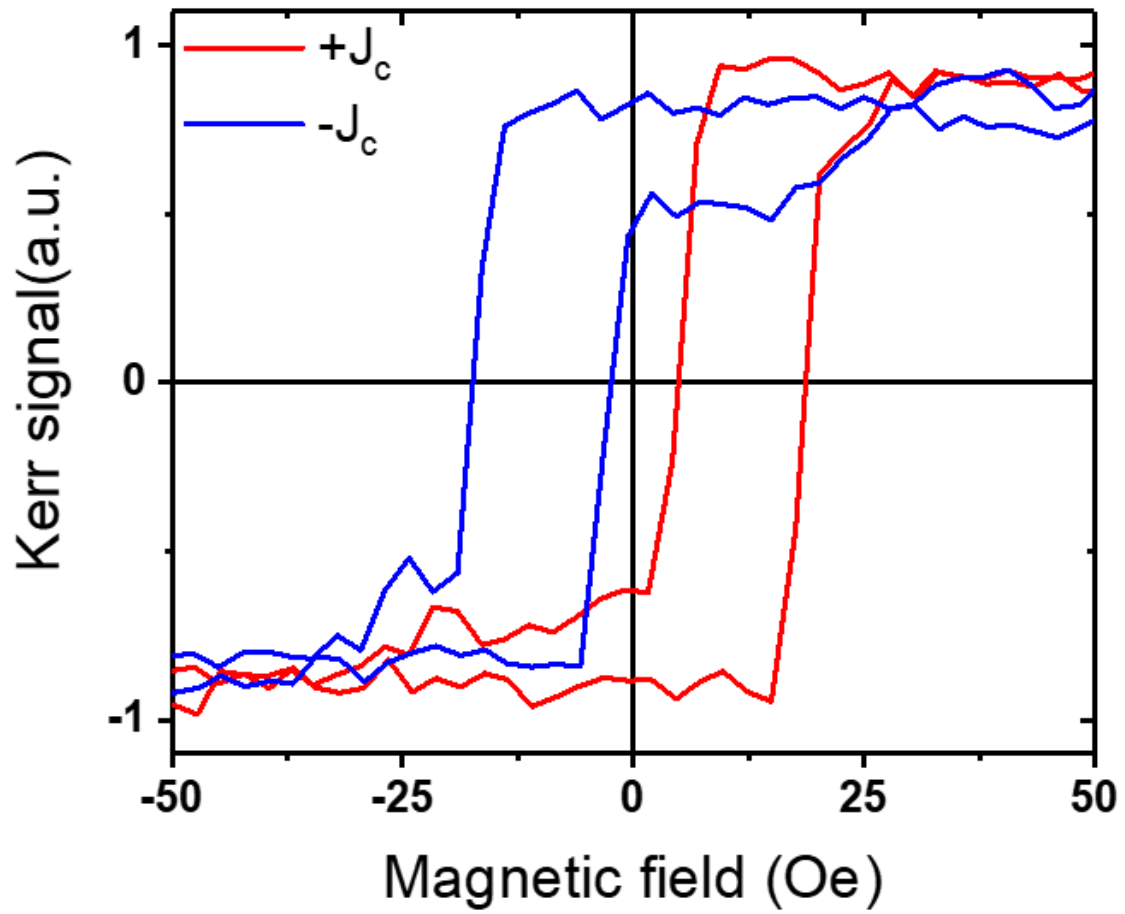


Fig. 29 Hysteresis loops of 82% oxidized $\text{Co}_{0.7}\text{-Ni}_{0.3}\text{-O-Pt}$ phase alloy single layer when current is applied, $J_c = \pm 4.2 \times 10^{10} \text{ A/m}^2$. Magnetic moment is aligned in same direction by induced exchange bias at H_{ext} is zero regardless of sweeping direction.

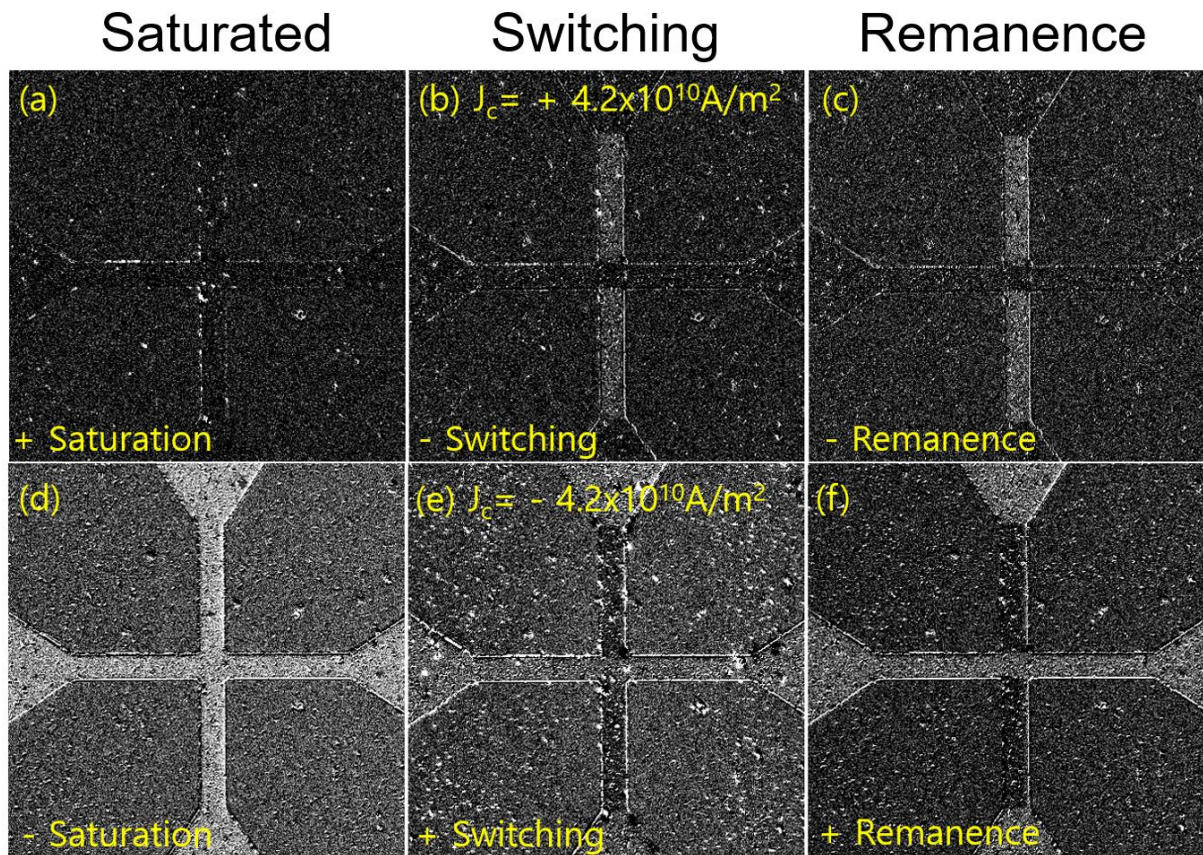


Fig. 30 Magnetic domain images. (a) and (d) are saturated by external field in \pm direction before applying current, (b) and (e) are switched by spin torque caused by spin Hall effect in opposite directions. (c) and (f) represent remanence magnetization formed in the switched direction.

IV. Conclusion

In this thesis, the Co_{0.7}Ni_{0.3}O-Pt phase alloy single layer having a structure in which each phase is randomly distributed in several nanometer sizes like the alloy was reported. When current was applied to this material, the spin structure of the AFM phase was controlled by spin torque caused by spin Hall effect, which was reflected as the exchange bias. Also magnitude of induced exchange bias is proportional to current density and oxidation degree of films. Induced exchange bias showed stable reversibility and repeatability, which was found at all measured current densities. In addition, field-free magnetization switching was possible through induced exchange bias, and the required current is remarkably one order lower than the reported one, $J_c \sim 10^{10} \text{A/m}^2$. We suggest that it will be utilized effectively in the field of spintronics through low current density and stability.

VI. Reference

- [1] Piramanayagam, S. N. (2007). Perpendicular recording media for hard disk drives. *Journal of Applied Physics*, 102(1), 2.
- [2] Tehrani, S., Slaughter, J. M., Chen, E., Durlam, M., Shi, J., & DeHerren, M. (1999). Progress and outlook for MRAM technology. *IEEE Transactions on Magnetics*, 35(5), 2814-2819.
- [3] Apalkov, D., Khvalkovskiy, A., Watts, S., Nikitin, V., Tang, X., Lottis, D., ... & Driskill-Smith, A. (2013). Spin-transfer torque magnetic random access memory (STT-MRAM). *ACM Journal on Emerging Technologies in Computing Systems (JETC)*, 9(2), 1-35.
- [4] Liu, L., Moriyama, T., Ralph, D. C., & Buhrman, R. A. (2011). Spin-torque ferromagnetic resonance induced by the spin Hall effect. *Physical review letters*, 106(3), 036601.
- [5] Liu, L., Lee, O. J., Gudmundsen, T. J., Ralph, D. C., & Buhrman, R. A. (2012). Current-induced switching of perpendicularly magnetized magnetic layers using spin torque from the spin Hall effect. *Physical review letters*, 109(9), 096602.
- [6] Miron, I. M., Gaudin, G., Auffret, S., Rodmacq, B., Schuhl, A., Pizzini, S., ... & Gambardella, P. (2010). Current-driven spin torque induced by the Rashba effect in a ferromagnetic metal layer. *Nature materials*, 9(3), 230-234.
- [7] Kong, W. J., Ji, Y. R., Zhang, X., Wu, H., Zhang, Q. T., Yuan, Z. H., ... & Naganuma, H. (2016). Field-free spin Hall effect driven magnetization switching in Pd/Co/IrMn exchange coupling system. *Applied Physics Letters*, 109(13), 132402.

- [8] Liu, Y., Zhou, B., & Zhu, J. G. J. (2019). Field-free magnetization switching by utilizing the spin Hall effect and interlayer exchange coupling of iridium. *Scientific reports*, 9(1), 1-7.
- [9] Moriyama, T., Oda, K., Ohkochi, T., Kimata, M., & Ono, T. (2018). Spin torque control of antiferromagnetic moments in NiO. *Scientific reports*, 8(1), 1-6.
- [10] Železný, J., Wadley, P., Olejník, K., Hoffmann, A., & Ohno, H. (2018). Spin transport and spin torque in antiferromagnetic devices. *Nature Physics*, 14(3), 220-228.
- [11] Liu, L., Pai, C. F., Li, Y., Tseng, H. W., Ralph, D. C., & Buhrman, R. A. (2012). Spin-torque switching with the giant spin Hall effect of tantalum. *Science*, 336(6081), 555-558.
- [12] Pai, C. F., Liu, L., Li, Y., Tseng, H. W., Ralph, D. C., & Buhrman, R. A. (2012). Spin transfer torque devices utilizing the giant spin Hall effect of tungsten. *Applied Physics Letters*, 101(12), 122404.
- [13] Marshall, W. (1955). Antiferromagnetism. *Proceedings of the Royal Society of London. Series A. Mathematical and Physical Sciences*, 232(1188), 48-68.
- [14] Shiino, T., Oh, S. H., Haney, P. M., Lee, S. W., Go, G., Park, B. G., & Lee, K. J. (2016). Antiferromagnetic domain wall motion driven by spin-orbit torques. *Physical review letters*, 117(8), 087203.
- [15] Hirsch, J. E. (1999). Spin hall effect. *Physical Review Letters*, 83(9), 1834.
- [16] Sinova, J., Culcer, D., Niu, Q., Sinitsyn, N. A., Jungwirth, T., & MacDonald, A. H. (2004). Universal intrinsic spin Hall effect. *Physical review letters*, 92(12), 126603.
- [17] Manchon, A., & Zhang, S. (2009). Theory of spin torque due to spin-orbit coupling. *Physical Review B*, 79(9), 094422.
- [18] Wang, B. M., Liu, Y., Ren, P., Xia, B., Ruan, K. B., Yi, J. B., ... & Wang, L. (2011). Large exchange bias after zero-field cooling from an unmagnetized state. *Physical review letters*, 106(7), 077203.

- [19] Zhu, W., Seve, L., Sears, R., Sinkovic, B., & Parkin, S. S. P. (2001). Field cooling induced changes in the antiferromagnetic structure of NiO films. *Physical review letters*, 86(23), 5389.
- [20] Nogués, J., & Schuller, I. K. (1999). Exchange bias. *Journal of Magnetism and Magnetic Materials*, 192(2), 203-232.
- [21] Wei, Z., Sharma, A., Nunez, A. S., Haney, P. M., Duine, R. A., Bass, J., ... & Tsoi, M. (2007). Changing exchange bias in spin valves with an electric current. *Physical review letters*, 98(11), 116603.
- [22] Stamm, C., Murer, C., Berritta, M., Feng, J., Gabureac, M., Oppeneer, P. M., & Gambardella, P. (2017). Magneto-optical detection of the spin Hall effect in Pt and W thin films. *Physical review letters*, 119(8), 087203.
- [23] Jung, M. S., Im, M. Y., Lee, B. H., Kim, N., Lee, K. S., & Hong, J. I. (2017). Magnetism of the hypo-oxide state at the diffuse interface between the ferromagnet and antiferromagnet phases. *Nanoscale*, 9(37), 14023-14030.
- [24] Jung, M. S., Kim, T. H., Im, M. Y., & Hong, J. I. (2020). Overcoming the limits of exchange bias effect in the magnetic thin films by introducing nanostructured internal interfaces. *Journal of Magnetism and Magnetic Materials*, 494, 165814.
- [25] Peng, X., Yang, Y., Singh, R. R., Savrasov, S. Y., & Yu, D. (2016). Spin generation via bulk spin current in three-dimensional topological insulators. *Nature communications*, 7(1), 1-9.
- [26] Feng, Y. P., Shen, L., Yang, M., Wang, A., Zeng, M., Wu, Q., ... & Chang, C. R. (2017). Prospects of spintronics based on 2D materials. *Wiley Interdisciplinary Reviews: Computational Molecular Science*, 7(5), e1313.
- [27] Patterson, A. L. (1939). The Scherrer formula for X-ray particle size

determination. *Physical review*, 56(10), 978.

[28] Yamamoto, S., & Matsuda, I. (2017). Measurement of the resonant magneto-optical kerr effect using a free electron laser. *Applied Sciences*, 7(7), 662.

요 약 문

Co_{0.7}-Ni_{0.3}-O-Pt 상 합금 단층에서의 스핀 토크(spin torque)에 의한 자계에 무관한 자화 반전과 교환 바이어스 유도

본 논문에서는 자성 단일층 박막 내의 합금과 같이 수 나노미터 크기의 상들이 무작위로 분포된 구조를 갖는 Co_{0.7}-Ni_{0.3}-O-Pt 상 합금 단층을 보고하였다. 일반적인 층간 박막 시스템과 달리 해당 구조는 단일층 내에 Co, Ni, O 그리고 Pt 상들이 무작위로 분포되어 독특한 계면 구조를 갖는다.

이 박막에 전류를 인가하였을 때 Pt 상에 흐르는 전류에 의해 발생한 스핀 홀 효과가 계면에서 다른 상들에 스핀 토크를 가하며 이 결과는 교환 바이어스의 변화를 통해 관측되었다. 발생 원인을 규명하기 위해 Pt 대신 Au 그리고 Co 과 Ni 대신 Fe 을 사용하여 동일한 구조를 제작하고 같은 실험을 진행한 결과 반강자성체의 스핀 구조가 스핀 홀 효과에 의해 조절되었음이 밝혀졌다. 또한 유도된 교환 바이어스의 크기는 필름의 전류 밀도 및 산화 정도에 비례하고 측정된 전류 밀도 범위 내에서 안정적인 반전성과 반복성을 띄었다. 이를 활용하여 외부 자계에 의존하지 않는 자화 스위칭 실험이 가능하였으며 이러한 현상은 모두 이미 보고된 결과보다 한 오더 낮은 전류 밀도인 $J_c \sim 10^{10} \text{A/m}^2$ 에서 이루어졌다.

따라서 본 논문의 연구 결과는 층간 박막 시스템이 가진 한계를 단일 박막층으로 제작된 구조를 통해 극복하였으며 이는 스핀 구조의 제어를 기반으로 설계된 디바이스의 성능을 향상시킬 가능성을 제시하였다.

핵심어: 스핀 토크, 스핀 홀 효과, 스위칭